Application of foam flooding for residual oil production in the “X” oilfield

by Stepan Verendeyev

Thesis supervisor: Dr. Randy Doyle Hazlett

Thesis co-supervisor: Dr. Sotirios Longinos

Thesis submitted to the School of Mining and Geosciences of Nazarbayev University in Partial Fulfilment of the Requirements for the Degree of
Master of Science in Petroleum Engineering

Nazarbayev University
29/04/2025

ORIGINALITY STATEMENT

I, Stepan Verendeyev, hereby declare that this submission is my own work and to the best of my knowledge it contains no materials previously published or written by another person, or substantial proportions of material which have been accepted for the award of any other degree or diploma at Nazarbayev University or any other educational institution, except where due acknowledgement is made in the thesis.

Any contribution made to the research by others, with whom I have worked at NU or elsewhere is explicitly acknowledged in the thesis.

I also declare that the intellectual content of this thesis is the product of my own work, except to the extent that assistance from others in the project's design and conception or in style, presentation and linguistic expression is acknowledged.

Signed on __/04/2025

ABSTRACT

Foam is a known diverting agent capable of improving sweep efficiency. It is speculated that foam flooding can also improve microscopic displacement efficiency in the reservoir core by the same mechanism. Recovery of trapped residual hydrocarbon fluid in the oilfield "X" core is investigated in this thesis. To quantify the recovery of bypassed resources on the core level, the application of foam flooding was investigated in the reservoir core and contrasted with the same recovery process sequence on homogeneous sandstone and carbonate quarried outcrop core. The study was the first to identify promising foam formulations using atmospheric bulk foam stability tests and use such foaming formulations with and without nanoparticle addition in immiscible core flood tests with nitrogen (N_2) and carbon dioxide (CO_2) carrier fluids.

Screening experiments of bulk foam stability were conducted as a precursor to core flooding studies. Foam half-life tests substantiated a negative influence of increasing salinity (NaCl) on foam stability. Appropriate baseline production from sequential water flooding and gas flooding preceded foam flooding assessments with both nitrogen and carbon dioxide gas options. Such tests were conducted in both reservoir and outcrop cores. Oil recovery and resistance factor observations were compared between reservoir and outcrop core, N_2 and CO_2 gas, and foam formulations with and without nanoparticle addition.

The X oilfield experiments confirmed significant EOR potential with foam processes, especially by adding nanoparticles. Baseline studies on gas flooding prior to foam introduction showed that CO_2 gas flooding is more efficient than N_2 flooding, even at low pressure, presumably due to the presence of additional interaction mechanisms with CO_2. Whether nanoparticles were present or not, the data showed that N_2 foam was more efficient than CO_2 foam, as evidenced by higher Recovery-8.15 % of Original Oil in Place (OOIP) with N_2 foam in "X" core samples compared to 2.45 % with CO_2 foam. Moreover, recovery was improved with the addition of NP to the foam formulation, resulting in an average additional recovery factor of 5.05%. However, the higher apparent viscosity of N_2 foam with nanoparticles (about 9 cP) must be carefully considered before field usage due to the associated mobility reduction, despite the dramatic increase in the recovery efficiency. In general, from the findings of this study, it appears that foam flooding is a feasible approach for enhancing sweep in the "X" oilfield.

DEDICATION

I dedicate this work to my mother, the person to whom I owe all of my achievements.

ACKNOWLEDGMENT

I would like to express my sincere appreciation to my supervisor, Professor Randy Hazlett, for his constant support, professional advice, and guidance during the writing of this thesis. His combination of in-depth knowledge and outstanding experience played a pivotal role in the success of this effort.

I am also incredibly appreciative of my co-supervisor, Dr. Sotirios Longinos, whose important counsel, direction, and mentoring have been crucial in defining my academic and personal development.

I also wish to thank my thesis committee members for their valuable comments and my research group for their unending assistance.

I am especially grateful to Dr. Azza Hashim Abbas (Grant No. 20122022) for providing the silica nanoparticles used in the experiments.

And I must thank Nazarbayev University School of Mining and Geoscience for the facilities, and a high quality environment to accomplish this work.

TABLE OF CONTENTS

LIST OF FIGURES

LIST OF TABLES

1. INTRODUCTION

1.1. Problem Definition

The oil production in oilfield "X," which started in 1980, is now nearing the end of its productive phase. A large amount of oil remains trapped within the reservoir's porous media (residual oil). Traditional water flooding methods have proven ineffective in recovering this oil due to the geological challenges presented by low matrix permeability and the presence of high-permeability channels. These issues limit the recovery factor (RF) and hinder further production.

1.2. Objectives

The objectives of this study are to:

- Introduce bulk foam screening criteria to determine the criteria for promising foaming formulations.
- Evaluate the stability of the foam under experimental conditions in porous media and its effectiveness in improving the recovery factor, particularly in cores with potential reservoir challenges, such as low matrix permeability and high-permeability channels.
- Demonstrate and quantify the improvement in microscopic displacement efficiency in one-dimensional core floods using foam flooding techniques.
- Compare the performance of reservoir cores with standard sandstone and carbonate outcrop materials.
- Compare the performance of nitrogen and carbon dioxide immiscible displacement with and without foaming agents.

1.3. Hypothesis

It is hypothesized that the foam used in core flooding will remain stable throughout the displacement process and will help to mobilize and recover the remaining oil trapped in the core. Additionally, the addition of nanoparticles to the foam formulation is expected to improve the foam stability and increase the overall recovery factor by reducing the mobility of the displacing fluid, thereby providing more uniform oil displacement.

2. LITERATURE REVIEW

2.1. Enhanced oil recovery

2.1.1. *Enhance oil recovery methods*

Enhanced Oil Recovery (EOR) is a set of advanced techniques designed to extract additional hydrocarbons from reservoirs after primary and secondary recovery methods have been applied. Primary methods use natural reservoir energy, while gas injection and waterflooding are common secondary methods that add energy to the system. Once secondary techniques become uneconomical, it is necessary to implement enhanced oil recovery (EOR) methods in order to further maximize oil recovery [2], [3]. The application of an Improved Oil Recovery (IOR) or EOR process to alter a declining oil rate in light of a defined Economic Limit (EL) is shown in Figure 1.

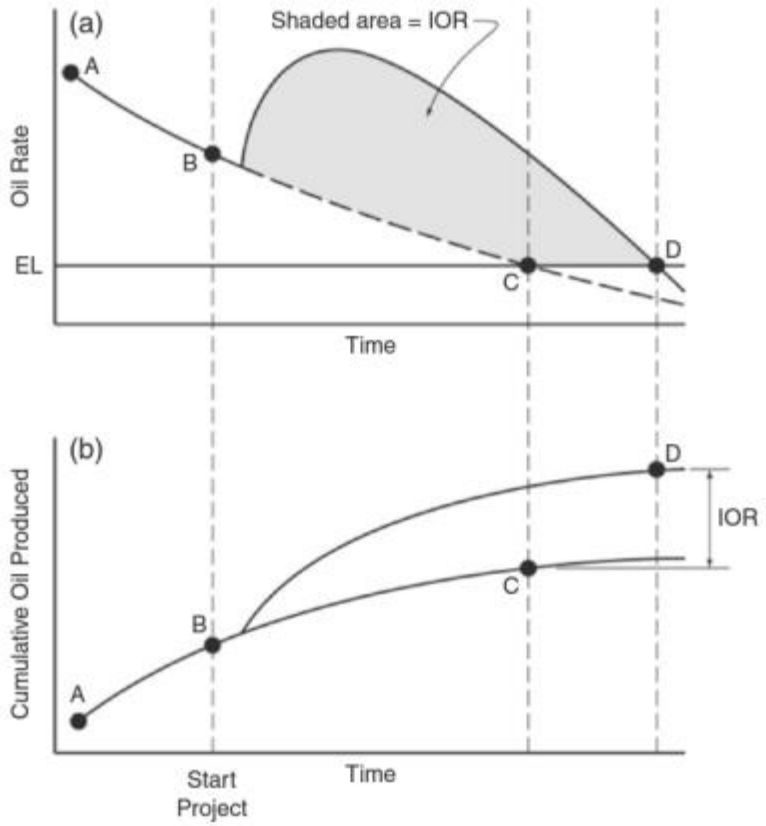

Figure 1 Schematic of IOR from typical EOR response: (a) rate vs. time and (b) cumulative vs time [3]

The three primary categories of EOR techniques are miscible gas, chemical, and thermal methods [6], as illustrated in Figure 2.

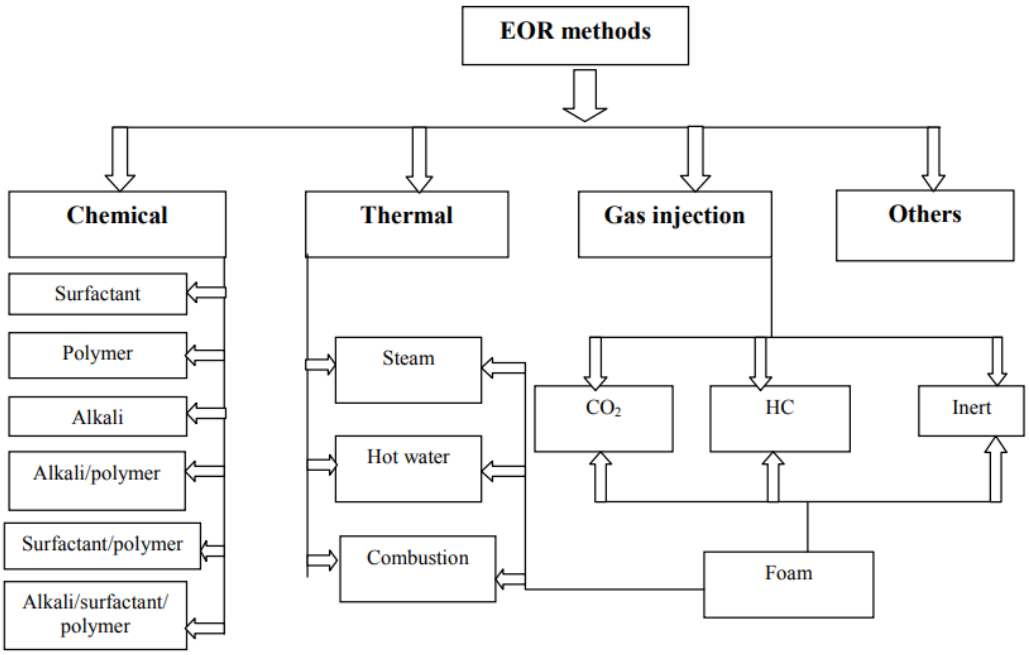

Figure 2 Simplified classification of EOR method [6]

The main objective of thermal techniques like in-situ combustion, steam flooding, and cyclic steam stimulation (CSS) is to decrease oil viscosity in order to increase its mobility within the reservoir [3]. Chemical EOR encompasses techniques such as alkali flooding, polymer flooding, surfactant flooding, and their combinations, e.g. Alkaline-Surfactant-Polymer (ASP) flooding. According to Sheng (2013) [5], these methods concentrate on improving sweep and displacement efficiency by changing the interfacial tension between water and oil. Miscible gas methods, such as carbon dioxide (CO_2) injection and hydrocarbon gas injection, involve introducing gases into the reservoir, which become miscible with oil either on first contact or through multiple extraction contacts with crude oil, substantially reducing oil viscosity and improving displacement efficiency [1][7]. The process is illustrated in Figure 3.

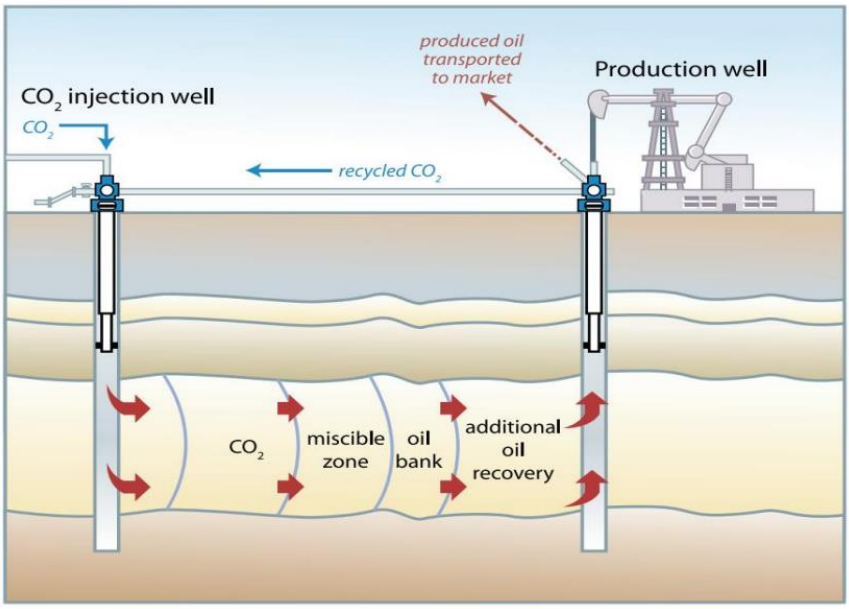

Figure 3. Miscible flooding technique principal scheme [7]

Chemical techniques have demonstrated significant promise in domains where environmental factors or reservoir temperature limitations make thermal techniques less attractive. Chemical EOR has attracted a lot of attention because of improvements in injection techniques and chemical formulation developments that have significantly raised its economic viability and efficiency [4].

2.1.2. *Foam injection*

Foam injection is a specialized chemical Enhanced Oil Recovery (EOR) method in which gas and surfactant solutions are injected into reservoir formations as foam. Foams, defined by a segmented gas phase in a continuous liquid phase stabilized by surfactants [9], significantly decrease gas mobility in porous media. In heterogeneous reservoirs with high permeability contrast or unfavorable mobility ratio, gas mobility control is advantageous, as foam enhances the mobility of injected fluids and enhances sweep and displacement efficiency [8].

The primary mechanism of foam flooding is the generation of a quasi-stable foam structure in reservoir pores, which reduces gas mobility to a large extent. Foam enhances the effective viscosity of injected gas to reduce gas channeling and viscous fingering, two recurrent issues seen in gas injection processes. Consequently, foam injection improves conformance control,

ensuring more homogeneous oil movement through the reservoir, as illustrated in Figure 4.

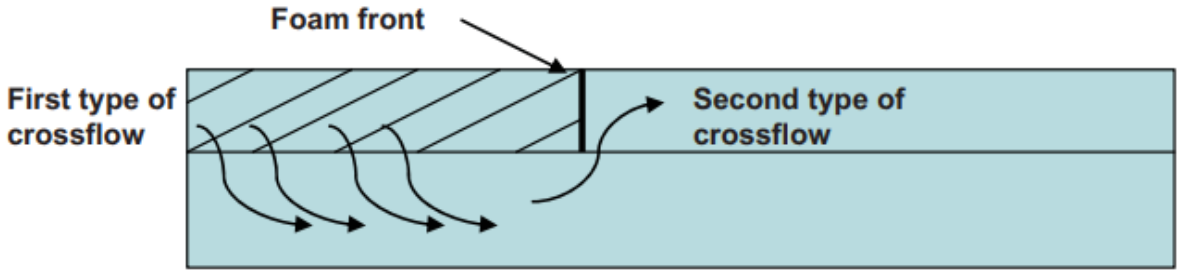

Figure 4 – Schematic illustrating two types of crossflow during foam flooding [12]

Foam stability is affected by several important factors such as surfactant type and concentration, gas composition, reservoir temperature and pressure, salinity, oil presence, and reservoir rock properties [10]. Laboratory studies and reservoir simulations are key before implementation, because optimal foam formulations are customized to specific reservoir characteristics. Nitrogen (N_2), carbon dioxide (CO_2), and, in some cases, hydrocarbon gases are commonly used for foam flooding, and their selection is dependent on operational economics and reservoir compatibility [18].

Selecting the appropriate surfactants which can provide long-lasting stability and desired interfacial properties at reservoir conditions is paramount for successful foam injection. The application of foam flooding technology has been broadened as a result of emerging developments in chemical formulations for improved performance in harsh environments, like high-temperature, high-salinity reservoirs [11].

Such fundamental concepts lay the groundwork for the subsequent analysis of foam injection applications in this section, which involves discussing the findings from the prior research and case studies.

2.1.3. *Field cases of foam injection*

Foam injection has been successfully implemented in several oilfields around the world, demonstrating its effectiveness in enhancing oil recovery. For example, results from the Snorre Field in Norway show that foam-assisted water-alternating-gas (FAWAG) techniques significantly improved the effectiveness of the sweep and conformance, which resulted in increased oil recovery [14]. In the United States, foam flooding was used successfully in Prudhoe Bay, Alaska, where injection of CO_2 foam increased oil recovery rates significantly, with reduced gas channeling and improved reservoir sweep efficiency [13].

While foam flooding is a proven technology elsewhere, there is still a strong research gap on the use of foam flooding for Kazakhstani reservoirs. There are no detailed case studies or explicit documentation of foam flooding implementations in Kazakhstan. Thus, this study was designed to fill this knowledge gap by evaluating the feasibility and effectiveness of foam flooding in Kazakhstan's oilfield X located in the Mangystau region. Overall, novelty of the current study is found in innovative analysis and applied assessment of foam injection in Kazakhstani reservoir core, which offers valuable knowledge and a methodological approach for potential broader regional implementation.

2.1.4. *Foam injection in EOR: results and case study insights*

Foam injection is an Enhanced Oil Recovery (EOR) technique that involves injecting a mixture of gases (e.g. CO_2, hydrocarbon gas, air, or steam) and surfactant to generate foam in the reservoir. This foam reduces gas mobility and diverts the flow into oil-rich zones, improving sweep efficiency. Over the past decades, numerous laboratory studies, field pilots, and simulations across the world have documented higher oil recovery, improved gas utilization, and viable economics with foam EOR. Major findings from global foam injection research, with verifiable sources from journals, industry reports, and conference papers were investigated and applied in the current research.

2.1.4.1. Sweep Efficiency increase

Many studies report significant incremental oil recovery when foam is applied, as foam blocks high-permeability “thief” zones and forces injectants into unswept regions:

North Sea (Snorre Field) – The largest foam-EOR project to date, foam was applied during a water-alternating-gas (WAG) flood to control gas breakthrough. No major operational issues were encountered, and oil production rates increased. The foam treatment produced an estimated 250,000 standard m^3 of additional oil, approximately 1.6 million barrels [18]. This showcases foam’s ability to recover substantial oil volumes by improving conformance in a mature offshore field.

Northeast China (Huanxiling Heavy Oilfield) – After conventional steam flooding had reached a 33 % recovery factor, nitrogen-foam injection was piloted to target remaining oil. Over a 33-

month pilot, foam recovered an extra 5.5 % of the original oil in place (OOIP). Scaling up to a 9-well pattern for 54 months yielded a total of 9.75 % OOIP incremental oil [18]. Notably, foam-injection wells showed higher injectivity and oil rates than waterflood wells, indicating foam can boost production even after water/steam flooding cycles [18]. This case demonstrated foam's effectiveness in heavy oil EOR, beyond traditional gas floods.

Colombia (Cusiana Field, Volatile Oil Reservoir) – In a mature gas-injection project with high gas-oil ratios, a surfactant-alternating-gas (SAG) foam pilot was conducted in one injector well. Within 2–3 months of foam injection, oil rates in connected producers increased (or decline rates flattened) and GOR dropped in three offset wells [16]. The incremental oil due to foam in the first cycle was about 30,000 STB [16]. Although modest in volume, this was achieved in a high-recovery, late-life reservoir.

United States (CO_2 Foam Floods) – Field pilots in CO_2-flooded reservoirs have consistently shown improved sweep and additional oil when foam is used for mobility control. For example, a Denbury Resources CO_2 flood pilot on the U.S. Gulf Coast used foam to remediate a high-permeability zone. In one producer well, GOR was cut by nearly 4 times and oil output more than doubled during foam injection, with benefits lasting well beyond the pilot period [22]. Across the pilot pattern, oil production was maintained while GOR fell, greatly improving CO_2 utilization efficiency [22]. This translated into significant CO_2 savings (less recycled gas needed) and confirmed that foam can increase oil recovery by diverting CO_2 into previously bypassed zones [22]. Earlier CO_2-foam trials in the 1980s–90s (e.g. Rangely and North Ward-Estes fields in the USA) similarly documented reduced gas channeling and incremental oil [15], [20], laying the groundwork for today's larger-scale pilots.

2.1.4.2. Gas Mobility Control and Efficiency Improvements

A primary benefit of foam in EOR is its ability to drastically improve gas sweep efficiency and conformance:

Reduced Gas Channeling and GOR – Foam increases the resistance to flow in high-permeability streaks, delaying gas breakthrough and lowering produced GOR. In the Snorre

FAWAG project, injecting foam into a thief zone diverted gas to oil-saturated layers, resulting in a sustained oil rate uplift [18]. Processes compared are illustrated in Figure 5.

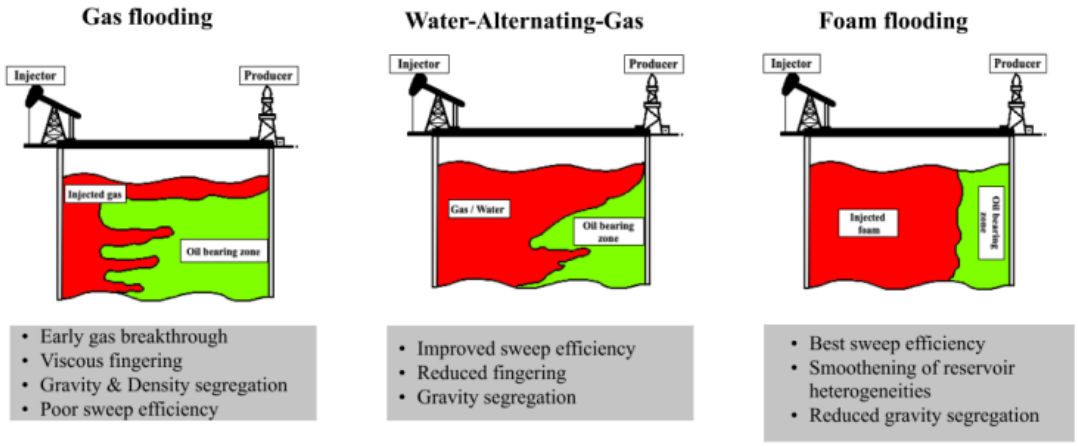

Figure 5 - Comparison of gas, water-alternating gas (WAG), and foam injections [18]

In the Denbury CO_2 flood pilot, wells that previously had to be shut in due to excessive GOR were able to produce with acceptable gas levels after foam treatment [18]. Across multiple pilots, foam has proven to constrain gas cycling – for example, CO_2 injectivity was intentionally reduced by 40–85 % in a West Texas foam trial, sharply cutting gas production in problem wells and improving overall flood efficiency [20]. By spreading CO_2 or injected gas more uniformly, foam increases the amount of oil contacted per unit of gas injected, making the EOR process more efficient.

Improved Sweep and Contacted Oil – By plugging high-flow pathways, foam forces the injectant to invade lower-permeability zones that contain remaining oil. Field logs in Colombia's Cusiana pilot confirmed that after foam injection, the target high-perm layer's share of gas flow dropped from 49 % to 17 %, indicating injection was diverted into previously bypassed layers [16]. This deep diversion of flow translated to new oil production, as evidenced by the temporary ramp-up in oil from surrounding wells [16]. In the Gulf Coast CO_2-foam pilot, average oil rates stayed constant (instead of declining) while using less gas, implying that foam pushed CO_2 into unswept pockets of the reservoir to liberate additional oil [22]. Overall, foam's mobility control leads to more uniform sweep of the reservoir, addressing a common shortcoming of gas injection EOR (which often leaves heterogeneities under-swept) [22].

Higher Post-Flood Recovery Factors – Several foam projects achieved notable increases in final recovery. The Chinese heavy oil pilot reached nearly 10 % of OOIP extra recovery beyond what steam flood alone accomplished [18]. In the North Sea, implementing foam after waterflood and initial WAG added 250,000 standard cubic meter of oil that would have been otherwise unrecovered [18]. These case studies underscore a trend: foam injection can extend the productive life of a flood and capture incremental oil once conventional methods plateau.

2.1.4.3. Operational Feasibility and Economic Considerations

Research and field experience indicate that foam EOR can be practically implemented and economically beneficial under the right conditions:

Operational Success in the Field – Foam injection has proven operationally feasible in diverse settings (offshore platforms, onshore fields, deep wells with high temperature, etc.). For instance, the Snorre FAWAG pilot was executed offshore with no major issues [18], and the onshore Cusiana SAG foam was pumped via coiled tubing into a deep, high-pressure well without incident [16]. After foam treatments, injectors generally recover their injectivity within days to weeks, meaning the foam does not permanently damage the formation. In Cusiana, the injector well returned to its normal injection rate ~2 weeks post-treatment, confirming low risk of plugging the reservoir completely [16]. Such findings have built confidence that foam can be deployed safely and repeatedly if needed.

Cost Effectiveness and Gas Savings With the foam-based conformity control, it is also relatively less expensive and easier to implement than mechanical alternatives. Foam can be injected through existing wells, is relatively low-cost and has no potential to damage the reservoir, like gel plugs or well recompletions [22]. Field tests have demonstrated large CO_2 savings when foam and the gas were used for supplementary EOR operations [22]. By providing higher oil recovered per injected gas volume and reduced recycled gas [22], foam economizes costs in gas EOR surges. For example, air-foam injection is being investigated as a low-cost format of EOR, because air is abundant and unmetered. This choice of foam gas alone pushes economics up. The low cost of gas and the stimulating effect of foam to control mobility and air for low-medium oil oxidation makes air injection with foam economically

attractive in low-permeability reservoirs [17], this method is “more economical and feasible” for recovering remaining oil in a particular type of reservoir.

Good Project Economics: Several foam experiments have published good project economics or, at least, incremental oil behind the expense. The extra oil (millions of barrels) from the Snorre FAWAG project obviously outweighed the cost of the surfactant [18]. The operator in Colombia noted a potential way to "improve the economic value of the project" [16] by reducing operational complexity, such as not being overly selective in foam placement. With a well-selected candidate (high GOR issue, heterogeneous reservoir, etc.), the incremental oil revenue and/or gas cost savings usually balance the chemical and injection costs of a foam, allowing foam-EOR to be a profitable investment.

2.1.4.4. Emerging Trends in Foam EOR Research

The success of foam injection in many EOR contexts has led to continued research to improve foam performance and expand its use:

Nanoparticle stabilized foams: A major technical target is the enhancement of foam stability in challenging reservoir conditions. Adding nanoparticles (like silica and polymers) makes foam compositions more stable to high temperatures, salt, and oil presence [18]. Research shows irreversible adsorption of nanoparticles at gas-liquid interfaces can not only thicken foam films, but can delay coalescence, allowing the foam to survive longer in the reservoir [18]. Preliminary tests indicate that nanotechnology-injected foams have mobility control at greater depths into the formation, potentially benefiting EOR efficacy.

Broaden Applications: Researchers are exploring foam EOR in challenging and unconventional reservoirs. For example, a recent field pilot injected a hydrocarbon-based foam into a tight shale oil reservoir in an "industry-first" experiment to see whether foam can mobilize oil in "unconventional" formations [18]. Since foam may allow more CO_2 to be trapped in the formation during oil production, CO_2 storage (carbon sequestration) co-optimization is also being examined [22]. Additionally, hybrid foam processes combining low-tension polymers, alkaline compounds, or surfactants with foam are being explored to achieve simultaneous sweep conformance and mobilization of the residual oil [15], [18].

Global Adoption and Learnings: The foam-EOR research has been a truly global pursuit with contributions from North America, Europe, Asia and the Middle East. The Siggins Field test in Illinois in the 1970s and pilots in Canada, the US, Europe and China in the 1990s have yielded decades of best practices and lessons learned from the field [18]. This understanding has just begun to be applied by contemporary pilots to generate more effective foam injection (ideal surfactants, slug sizes, injection schedules), such as in the carbonate fields of Oman, the low-perm reservoirs of China and the mature fields of Latin America. In summary, this trend shows increasing confidence of foam EOR as a method to improve oil recovery while increasing the efficiency of gas flooding, making it both technically and economically viable.

2.2. Geologic Context

2.2.1. *Geological overview of oilfield "X"*

Oilfield "X", located in geologically complex and multifaceted states, represents a source of interest in the exploration and development of oil and gas resources. Since its discovery and the first geological discoveries made at the end of the 20th century, its deposit has attracted the attention of specialists distinguished by its reservoirs and structure. The "X" field plays an important role in the oil and gas sphere of Kazakhstan, which determines its uniqueness for the national energy sector. Based on detailed studies, including analysis of cores from field wells carried out in 2018, basic data on the structure, mineralogy and petrophysical characteristics of productive horizons were obtained. Core material with a total area of 180 meters from one well was carefully studied at the Center for Scientific Laboratory Research of the KazNIPImunaigas branch of KMG Engineering LLP, where standard and special core studies were carried out. During the study of this core, the following indicators were identified in the Table 1.

Table 1. reservoir technical properties [33]

Porosity (%)	**Permeability (μm²)**	**Grain density (g/cm³)**
5,14	0.0001 -0.0005	2.62 -2.71

The average porosity of the rocks is about 5.14 % to 5.47 %, indicating low porosity of the reservoirs. Permeability values range from 0.00014 to 0.00021 μm², highlighting the limited filtration properties of the rocks [33]. The density values of rock grains were found to be from 2.62 to 2.71 g/cm³, which indicates the predominance of heavy minerals [33]. These

characteristics and the results of special laboratory tests of the core emphasize the complexity of the geological structure of the field and the need for an integrated approach to its development and operation. Oilfield “X”, due to its unique features, is an important object for geological science and the oil and gas industry of Kazakhstan, providing new data for the research and development of such complex geological objects.

2.2.2. *Geological structure and lithology*

In the Mangyshlak region, deep wells uncovered marine gray sediments of late Paleozoic age, which demonstrate a complex material composition, a significant degree of secondary transformations and dislocation. These deposits are part of the folded base of the Turan platform and have undergone post-sedimentary transformations corresponding to the stages of deep

metagenesis and greenschist metamorphism [32]. For a visual representation of the geological structure and location of research wells in this area, the well map is representing in Figure 6.

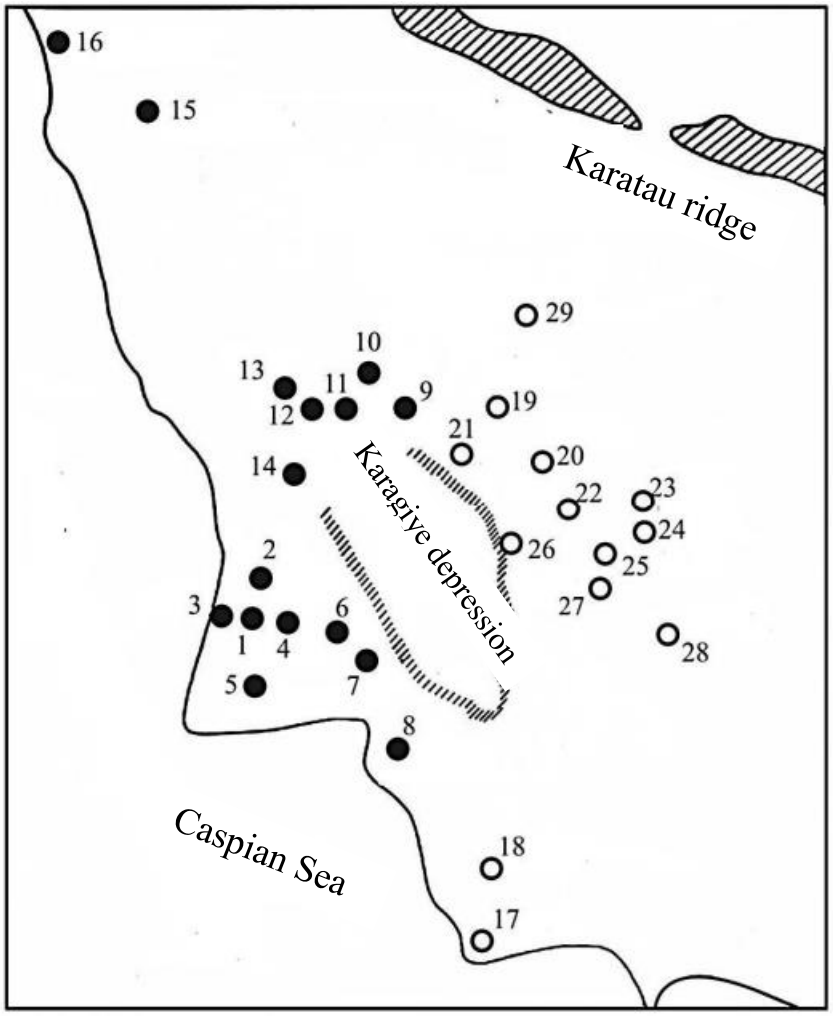

Figure 6. Mangyshlak Peninsula. Layout of areas,
on which the foundation is exposed by drilling.
Black circles are areas where rocks were exposed under Triassic sediments
lower structural tier of the foundation [32]

2.2.3. *Paleontological data*

The deposits have not been characterized paleontologically, but their position in the section, as well as the presence in the fragments of granite destruction products, the age of which in the

Oymashinskaya area is determined to be Carboniferous, allows us to assume their Late Paleozoic age [32].

2.2.4. *Tectonic features*

Paleozoic deposits of the Zhetybay-Uzen stage are characterized by the boundary conditions of metagenesis and early stages of greenschist metamorphism, which confirms their inclusion in the upper structural stage of the basement of the Turan platform [32].

The base of the Mesozoic deposits of Mangyshlak includes a dislocated Paleozoic basement with two main rock complexes: the lower, more highly metamorphosed, and the upper, which is lower molasse with Carboniferous-Early Permian spore-pollen complexes [32]. These data provide the basis for the development of new techniques for predicting and searching for minerals in this geologically complex region.

2.2.5. *Analysis of oil and gas potential*

In the context of the study published by Krupin (2011), special attention was paid to the study of the petroleum potential of the basement, especially granitoids, which represents a key aspect for assessing the prospects of the “X” field in comparison with similar geological structures of the world level. This analysis included an in-depth study of the lithological composition, textural features of the rocks and their geochemical characteristics. It is represented in geological profile along the line of wells 30-68-13 illustrated in Figure 7, made it possible to identify specific features characterizing high hydrocarbon potential [30].

It was found that the granitoids of the Field “X” deposit are characterized by a certain degree of metamorphization and changes caused by tectonic activity [30]. These processes have led to the formation of porous and fractured structures in rocks, which contribute to the accumulation

and preservation of hydrocarbons. An important aspect is the high level of permeability of these granitoids, which is a critical factor for the formation of effective hydrocarbon reservoir.

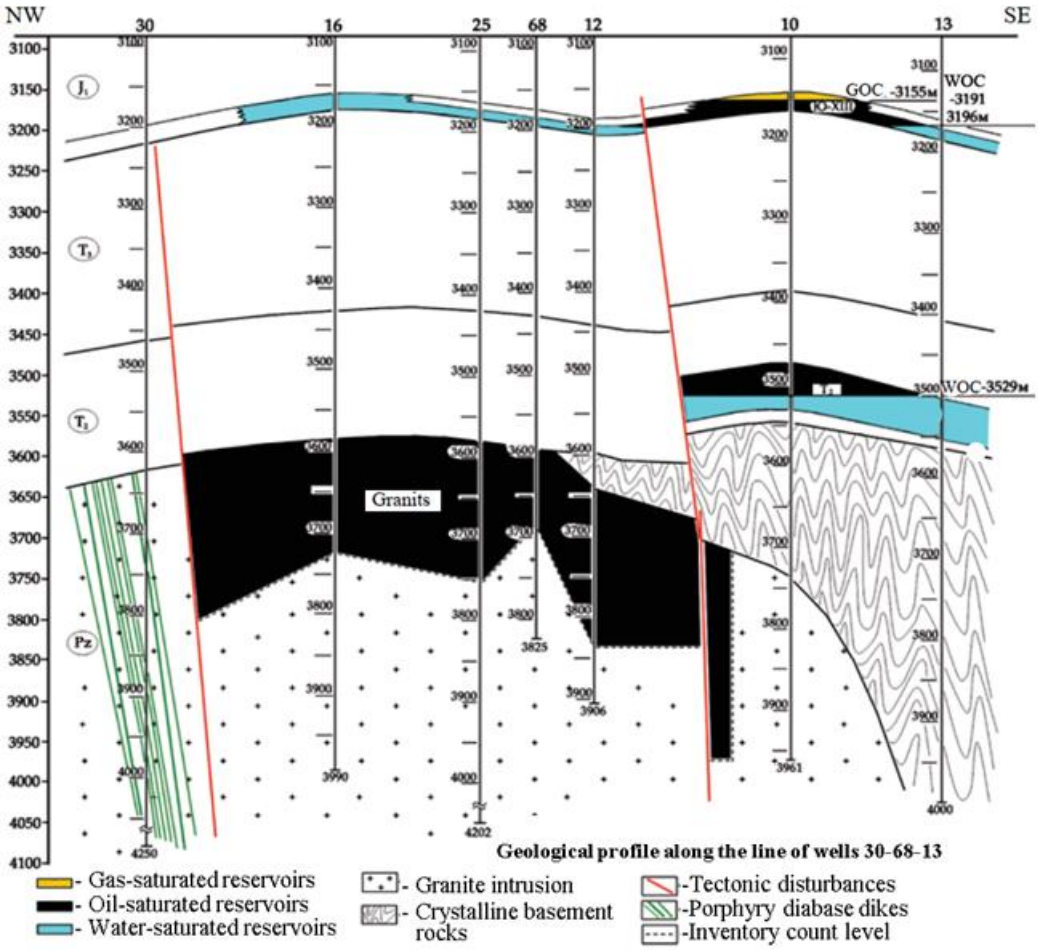

Figure 7. Geological profile along the line of wells 30-25-12-10-13 [30]

In addition, analysis of the organic carbon content in basement rocks indicates the presence of favorable conditions for the generation of hydrocarbons. Geochemical studies of the rocks confirm that the migration of hydrocarbons occurred under conditions conducive to their concentration in cracks and pores of granitoids, which in turn indicates the high potential of the oilfield “X” for oil and gas production.

The study also highlights the importance of understanding the geological history of the region and the influence of ancient tectonic events on the formation of the geological structure of the field. Comparison with data on other fields in the world showed that similar geological processes and conditions could contribute to the formation of similar hydrocarbon reserves in

granitoids, which makes the “X” oilfield a promising target for geological exploration and exploitation.

Thus, a detailed analysis of the oil and gas potential of the foundation at the “X” oilfield, based on a comparison of its geological, geochemical and tectonic characteristics with analogues in other parts of the world, demonstrates the significant potential of this deposit. Additionally, the study focuses on aspects such as granitoid depth, age and evolution, which together with geochemical data provide valuable information about the processes that led to the formation of potential hydrocarbon reserves.

One of the key points of the study is the analysis of the dynamics of hydrocarbon migration and the mechanisms of their accumulation in granitoids. The use of advanced methods in geochemistry and petrophysics has made it possible to clarify the migration paths of hydrocarbon flows in basement rocks, revealing the features of their distribution depending on the characteristics of fracturing and porosity of the rocks. These results highlight the importance of microstructural studies for understanding the potential of deposits in complex geological conditions.

2.2.6. *Structure of an oil reservoir in the granite massif of the “X” field*

The “X” oilfield, located in the south of Mangyshlak, is a unique example of an oil deposit in a granite massif. Based on long-term and field exploration, a reservoir model was developed that included granitoid intrusions as the main oil production target.

2.2.7. *Reservoir model and capacitive properties of granite massif*

Research has shown that the formation of the capacitive properties of a granite massif is controlled by a number of factors, including heat shrinkage and the tectonic-caisson effect. These processes promote the formation of fracturing and porosity in granite, making it an effective reservoir for oil accumulation. The article examines in detail the model of a reservoir in igneous rocks and offers recommendations for additional exploration of the deposit [31].

2.2.8. *Prospects for additional exploration of the field*

Modern methods of seismic exploration and interpretation of geological data, including CSP (Common Scattering Point) technology, have made it possible to identify new promising areas

in the basement granitoids and Middle Triassic carbonates. This data can significantly increase the efficiency of exploration for oil and gas-bearing reservoirs in the “X” field.

2.2.9. *Analysis of fractured-cavernous reservoirs*

The analysis carried out allows us to assert the existence of sheet-like areas of decompaction in the granite massif, which are the main reservoirs of oil. These zones are characterized by increased permeability and fracturing, which is confirmed by both drilling data and geophysical characteristics of the section: Figure 8 shows a model of an oil reservoir in the granite massif of the “X” area.

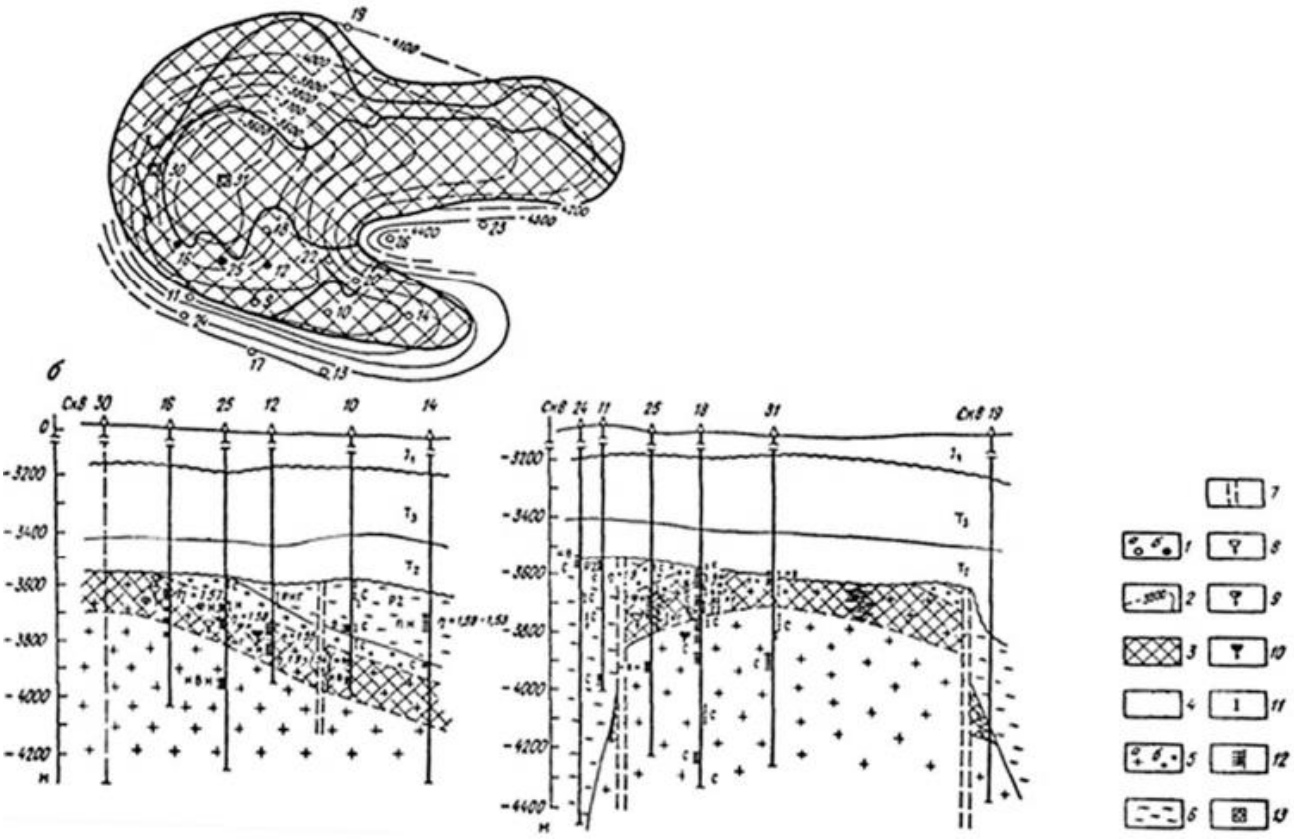

Figure 8. Model of an oil reservoir in the granite massif of the “X” area:
A – structural diagram of the reservoir in plan, B – geological sections, 1 – deep wells (a – exposed basement rocks, b – produced fountain inflows from granites); 2 – isohypsum on the roof of granites, m; zones: 3 – decompaction in granites associated with heat shrinkage phenomena, 4 – crushing associated with discontinuities; 5 – granites: a – coarse-crystalline, b – fine-crystalline; 6 – metamorphic rocks; 7 – discontinuities; drilling fluid absorption intervals: 8 – insignificant (10–15 m³/day), 9 – medium (from 10 to 40 m³/day), 10 – strong; 11 – open hole formation testing intervals, 12 – perforation intervals; 13 – wells under drilling or construction;
the nature of the resulting fluid according to IPG: N – oil, NV – oil and water, RNG – solution, oil and gas; character of the resulting fluid when tested in a column: PN - oil overflow, NVN - slight

influx of water from oil, FN – oil gusher; NV – minor influx of water, NN – minor influx of oil, NV – oil and water; C – layer “dry” [31]

Figure 9 shows a comparison of reflector and diffractor cubes imported into the interpretation project.

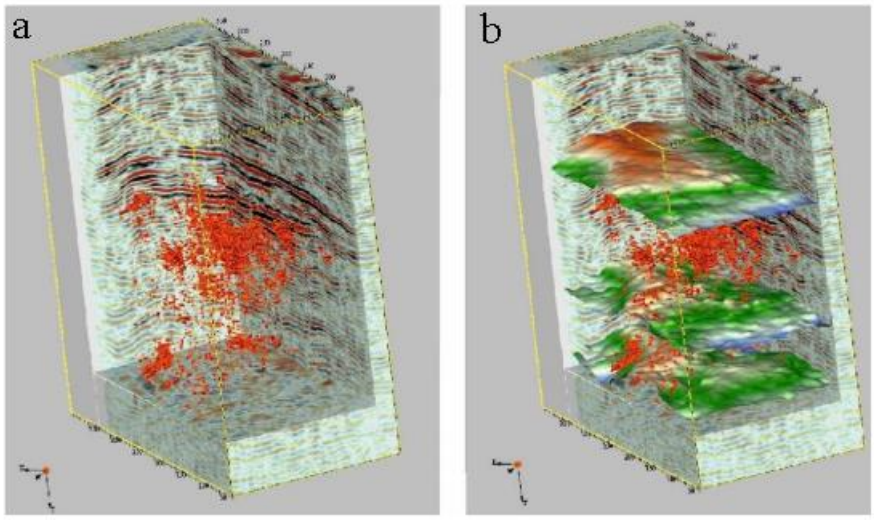

Figure 9. Comparison of cubes of reflectors and diffractors imported into the interpretation project: a) cube of reflectors and diffractors b) joint representation of cubes of reflectors and diffractors with isochronous surfaces along horizons V1, V2 and VI. [31]

Figure 10 presents a time slice of a cube of scattered waves across wells, which contributes to a deeper understanding of the distribution of fractured-cavernous reservoirs.

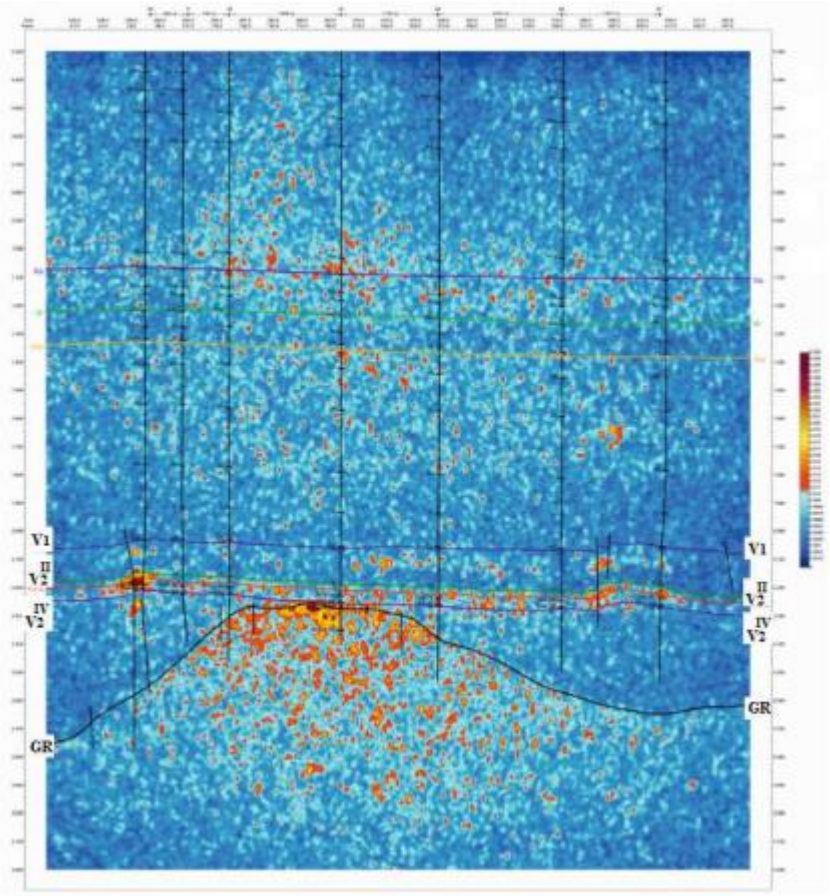

Figure 10. Time slice of a cube of scattered waves from wells 24-11-1E-22-27 [31]

Figure 11 shows a structural map of the top of the granite intrusion and a map of the oil and gas potential of the granite intrusion, highlighting the most promising areas for further exploration and development.

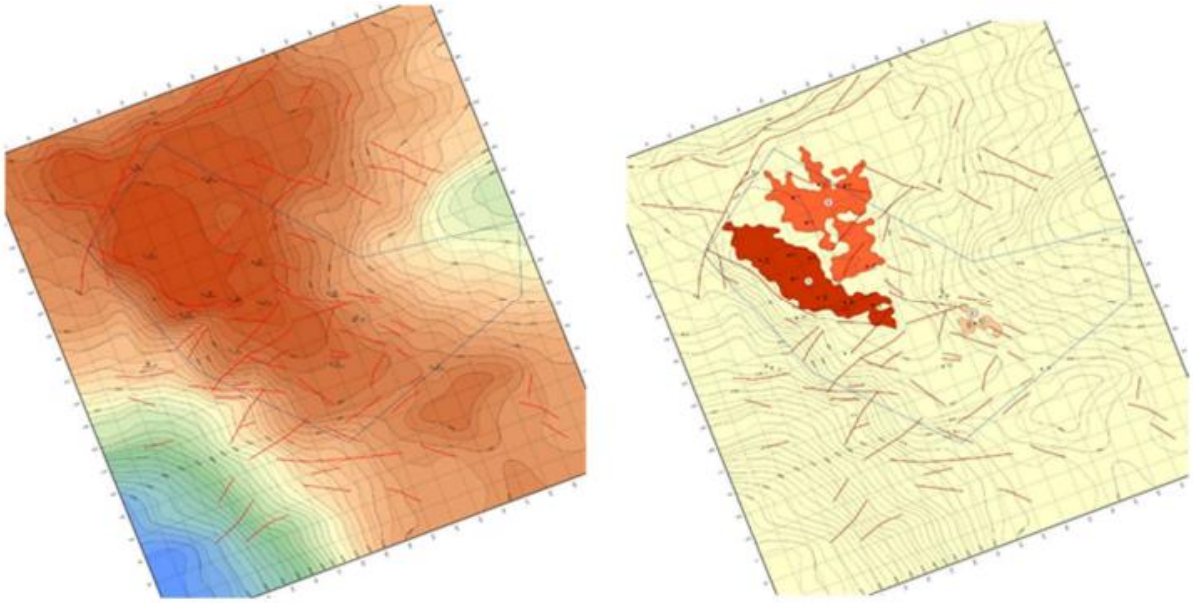

Figure 11. Structural map of the top of the granite intrusion (left) and prospect map (index acoustic heterogeneity) oil and gas potential of granite intrusion: dark red color on the map on the right – the most promising areas [31]

These illustrations are important for understanding the structure of the reservoir and confirm the hypothesis about the vein and reservoir nature of oil-bearing zones in the granite massif of the "X" oilfield.

2.2.10. *Fluid evaluation*

Assessing changes in the average values of fluid properties of productive horizons in the reservoir and surface conditions is a key aspect in the development of oil and gas fields. As part of this study, the properties of formation fluids of Triassic productive deposits of the "X" oilfield were analyzed. Analysis and comparison were carried out based on the results of studies of oil and gas samples, taking into account the parameters approved in the project documents. The study showed that oil from the "X" oilfield is characterized by high gas content and volumetric coefficient. The saturation pressure for the T_2 formation was 253 MPa, and for the granite intrusion - 189 MPa. Thermodynamic conditions of occurrence and high gas content contributed to the low density and viscosity of the reservoir oil. For example, in the Triassic the density was 0.715 g/cm³, and the viscosity was 0.42 mPa*s. Degassed oil of the Middle Triassic and granite intrusion shows a light composition, which led to low density and viscosity values, as well as a positive pour point. The density of oil from the T_2 horizon was estimated at 0.8365 g/cm³. The low content of asphalt-resinous substances with a high content of high molecular

weight paraffin hydrocarbons indicates the high quality of oil from the “X” oilfield. Gas from the “X” oilfield dissolved in oil is characterized by a high content of propane-hexane fractions and a significant content of ethane. Component analysis showed the presence of carbon dioxide in concentrations that differed from other deposits in the region. The results of studying the properties of reservoir fluids at the “X” oilfield confirm the high quality of oil and gas. Analysis data can be used to optimize the development and operation of the field, as well as to plan further research to improve the efficiency of hydrocarbon extraction.

2.2.11. *Well logs evaluation*

At the Center for Scientific Laboratory Research of KMG Engineering LLP "KazNIPImunaigas" standard and special comprehensive studies of core from the “X” oilfield were carried out [33]. The core material, totaling 180 meters in volume, underwent a comprehensive assessment including core acquisition, spectral gamma scanning, daylight and ultraviolet photo documentation, macroscopic characterization and selection of cylindrical samples for further analysis.

The use of an SPGL-300 spectral gamma scanner to analyze a 180-meter-long core provided data on the natural radioactivity of the rocks result that is presented in Figure 12. This stage made it possible to determine the content of thorium, potassium, and uranium in the rocks, which is key for further interpretation of the lithological composition.

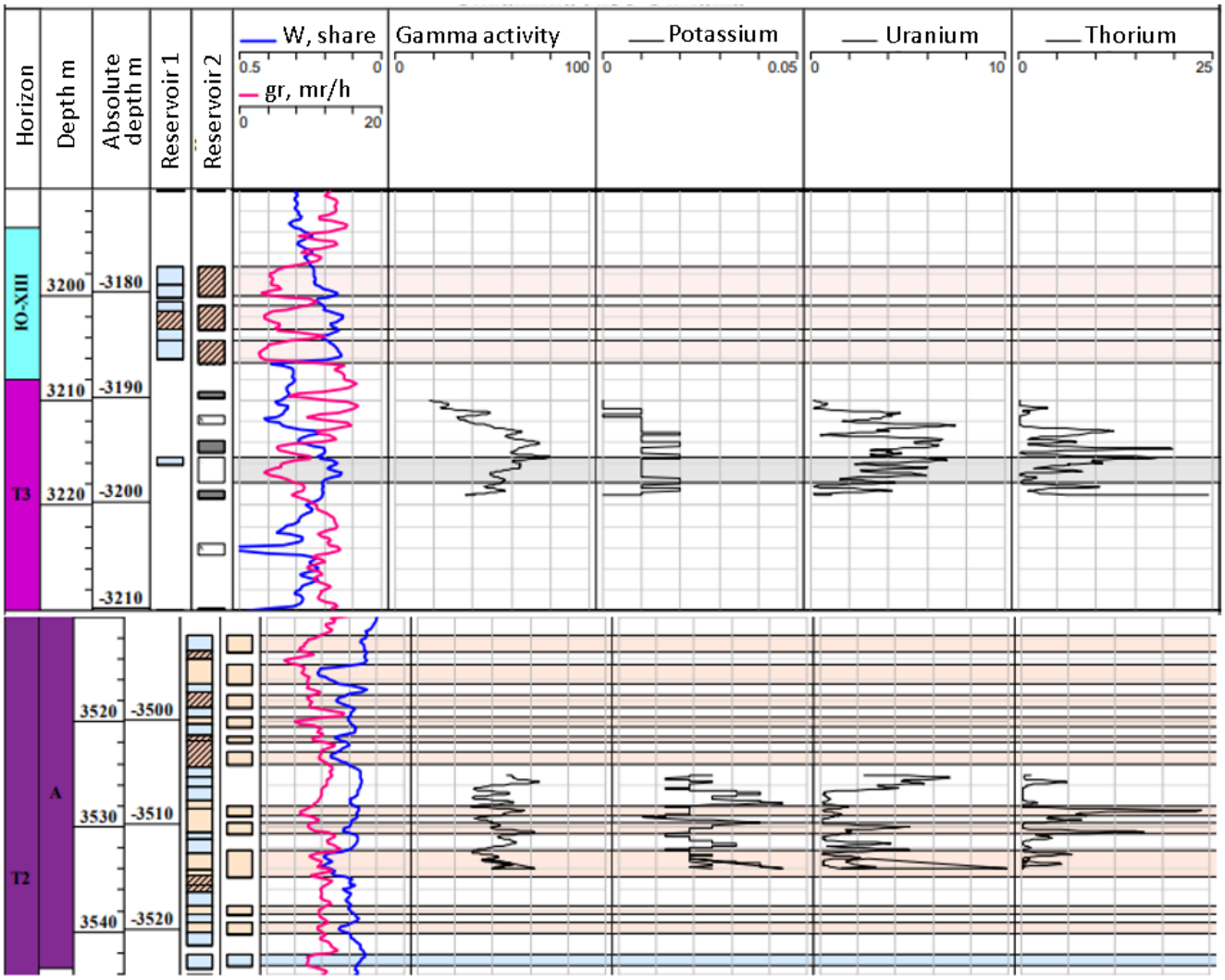

Figure 12 Results of spectral gamma-ray activity of a full-size core from the "X" oilfields well [33].

Photo documentation in Figure 13 provided visual evidence of the condition of the core, important for confirming macroscopic observations and lithological analysis.

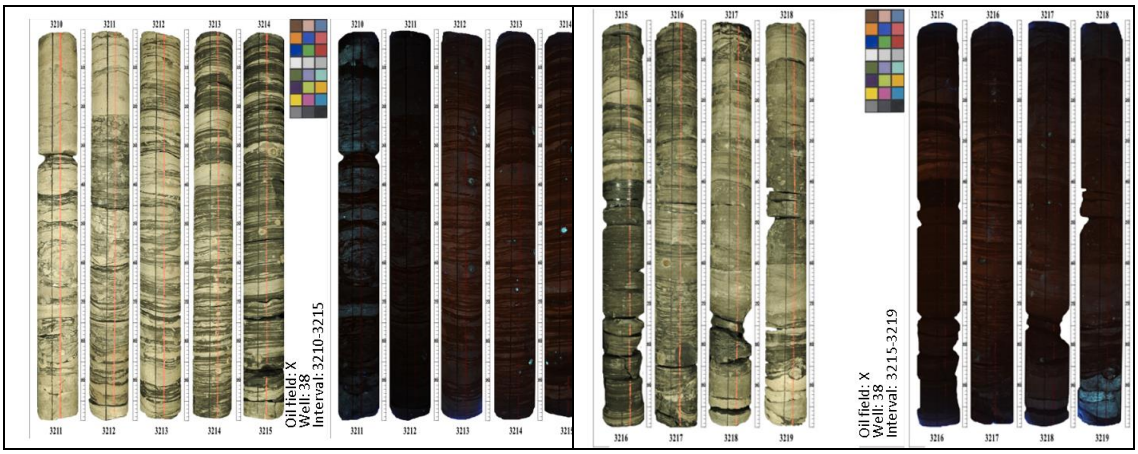

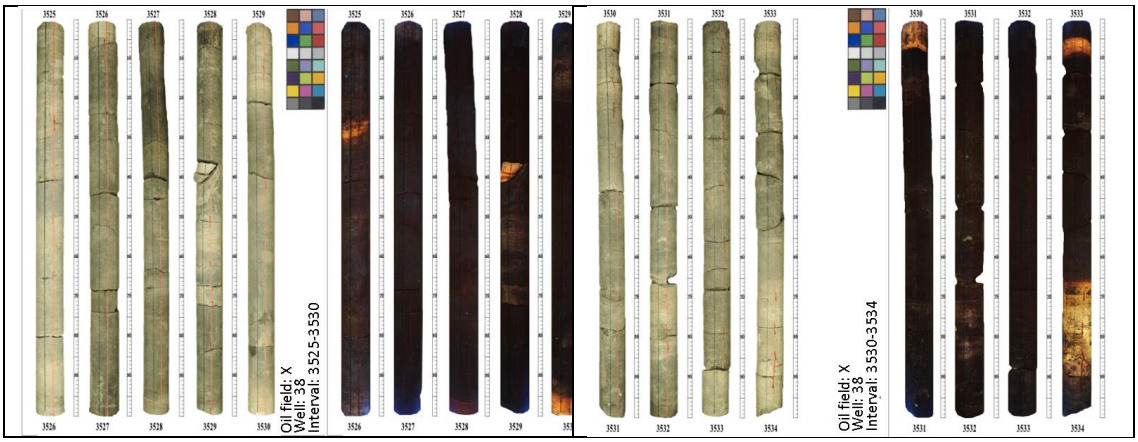

Figure 13. Results of photo documentation of core 1m-18m from "X" oilfield well [33].

As a result of the macroscopic description, the main types of rocks were identified: tuff sandstone, tuff siltstone, carbonaceous and micaceous siltstone, which indicates the diversity of sediments in this well interval. Standard laboratory tests of the core included determination of mineral density, porosity, permeability, carbonate content and lithological description of the samples. Research data confirms the high filtration and reservoir characteristics of the reservoir rocks of the "X" oilfield, which is the basis for optimizing further development of the field. The studies of core from the "X" oilfield demonstrate the complexity and diversity of the geological structure of the field. Data obtained from gamma ray spectral scanning, macroscopic characterization and standard laboratory analyzes provide valuable information for geological modeling and reservoir development.

2.2.12. *Core evaluation*

An in-depth study of core from well of the "X" oilfield were carried out on 82 cylindrical samples covering various depth intervals of the well. An UltraPoroPerm-500 device from Core Lab Instruments was used to determine the mineralogical density of grains, open porosity coefficients and absolute permeability of rocks using helium and nitrogen, respectively.

The determination of mineralogical density and open porosity by helium was carried out on a porosimeter of the UltraPorePerm 500 installation, where the volume of the mineral skeleton of the samples was determined using helium according to the Boyle-Mariotte law. The measurements made it possible to calculate the volumes of the mineral skeletons of the samples and, accordingly, their open porosity (Figure 14). The instrument calibration process was carried out immediately before measurements, ensuring the accuracy of the data obtained.

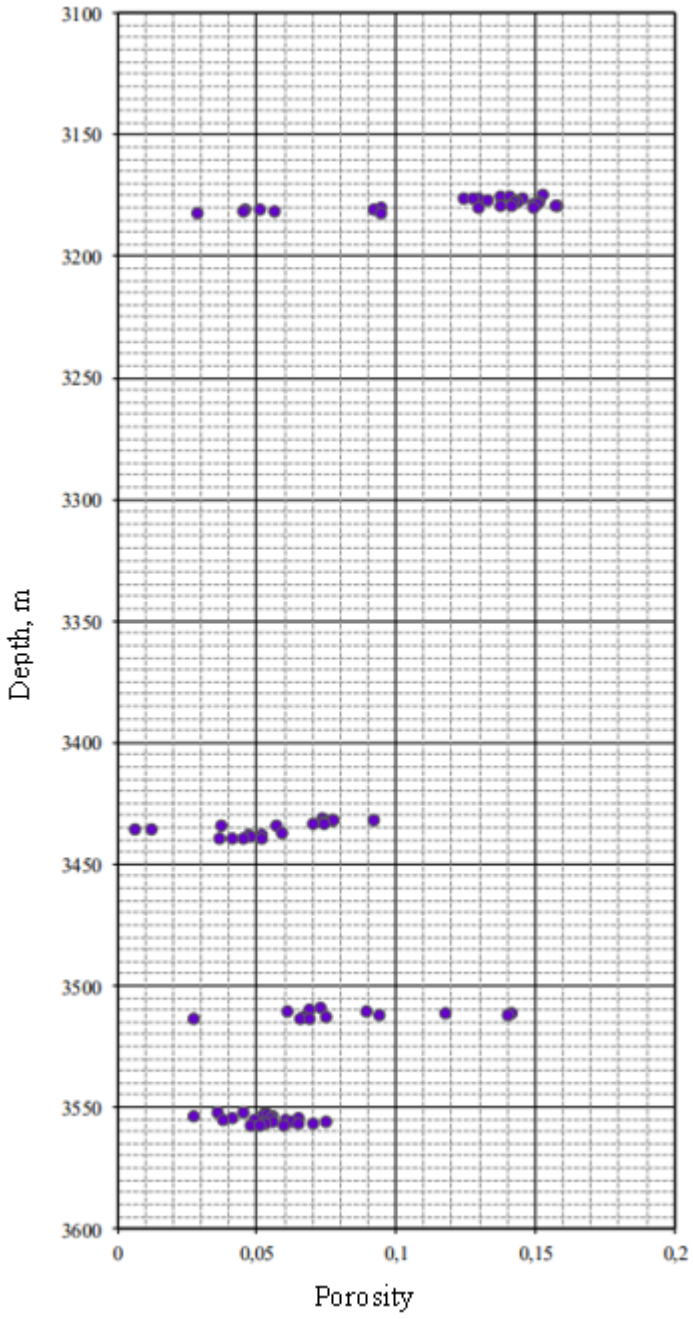

Figure 14. “X” oilfield well porosity distribution by depth

To determine the absolute permeability to nitrogen, the UltraPorePerm 500 permeameter was used. Core samples were placed in a Hassler core holder, on the side surface of which a hydrostatic pressure of 276 MPa was applied. The permeability of rocks to gas was calculated using the Darcy equation. These tests allowed us to evaluate the ability of rocks to transport gas through their structure (Figure15).

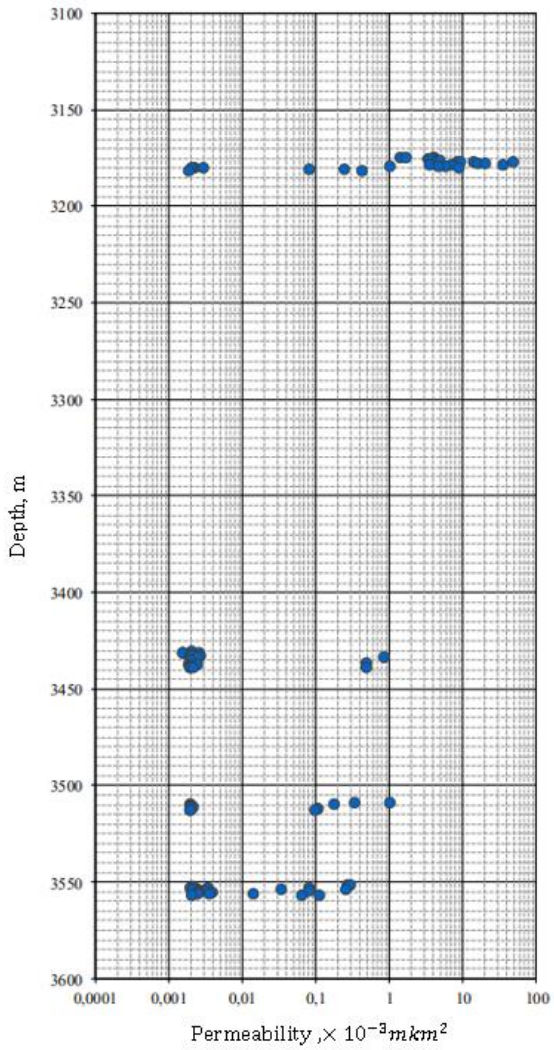

Figure 15. "X" oilfield well permeability distribution by depth

Detailed lithological descriptions of all 82 samples provided a comprehensive characterization of the studied rocks, including their textural and structural features, which is critical for geological analysis and interpretation of rock formation conditions. Standard and special studies of core from well of the "X" oilfield deposit provided valuable information on the mineralogical density, open porosity and absolute permeability of the studied rocks. The data obtained are of significant importance for further geological modeling of the field and planning its development.

2.2.13. *Hydrochemical water analysis*

As part of the hydrochemical analysis of water from well No. 68 of the "X" oilfield, a test was performed to determine the component composition of the water. The study was carried out in a hydrochemistry laboratory using standard analysis methods in accordance with GOST and other regulatory documents.

As a result of hydrochemical analysis, the following results were obtained: The pH value was 5.3, indicating an acidic reaction of the water (GOST 26449.1-85 clause 4). The measured density of water is 1.092 g/cm³ (GOST 18995.1-73). A high content of calcium (Ca^{2+}), magnesium (Mg^{2+}), the sum of potassium and sodium (Na^{+} + K^{+}), and chlorides (Cl^{-}) was determined, which indicates significant mineralization of the water. The calcium content was 98196 mg/dm³, magnesium - 15808 mg/dm³, the sum of potassium and sodium - 386630 mg/dm³, chlorides - 814290 mg/dm³. The calculated total salinity of the water reached 1317124 mg/dm³, highlighting the high degree of salinity. Defined as Cl-Ca, which characterizes the water as calcium chloride. Calculated at 6200 mEq/L, which indicates high water hardness.

Table 2. Hydrochemical analysis of water from well of the "X" oilfield

pH	5.3
Density	1.092 g/cm³
Mineral composition	The calcium content was 98196 mg/dm³, magnesi 15808 mg/dm³, the sum of potassium and sodiur 386630 mg/dm³, chlorides - 814290 mg/dm³
Total mineralization	1317124 mg/dm³
Total water hardness	6200 mEq/l

The results of hydrochemical analysis of water from well of the "X" oilfield demonstrate high mineralization and water hardness, which has significant consequences for the design of water treatment and drainage systems during field development. The Cl-Ca water type emphasizes the predominance of chloride and calcium in the mineral composition, which is an important factor in the analysis of water corrosivity and the selection of equipment materials.

An important element of the analysis is the study of changes in groundwater salinity with depth, which is visually presented in Figure 16 of the article. This graph not only clearly illustrates the increase in water salinity as one goes deeper into the earth's crust, but also emphasizes the complex relationship between geological processes and the hydrochemical composition of formation waters. The figure 10 clearly shows how water salinity gradually increases in the upper layers, which may be due to the penetration of surface water and its interaction with

rocks. However, in deeper layers, in particular in pre-Jurassic sediments, there is a sharp change in this trend. This indicates the presence of other processes affecting the composition of formation waters, such as deep degassing of the Earth and volcanic activity, which can introduce rare and valuable elements into the waters [34].

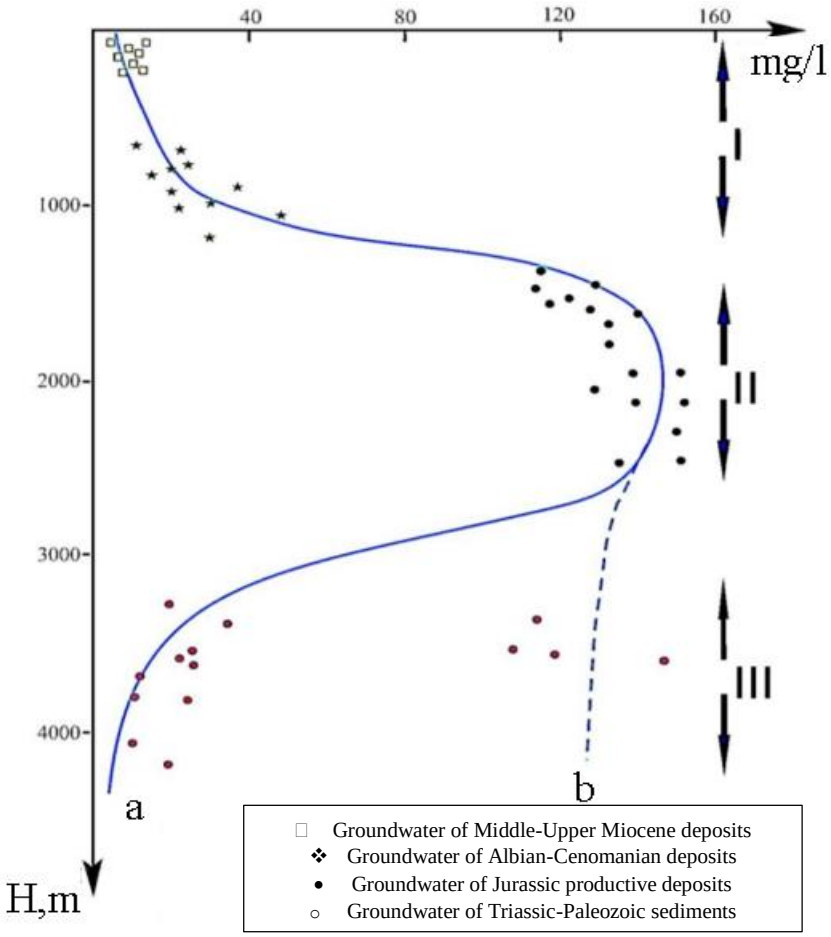

Figure 16. "X" deposit. Changes in groundwater salinity with depth [34]

2.2.14. *Geological report*

The "X" oilfield, with its unique geological structure and complex of geophysical, hydrochemical and petrophysical characteristics, is of significant interest to both the geological community and the oil and gas industry. The variety of studies and analyzes carried out emphasizes the complexity and multifaceted nature of the object under study, requiring a multidisciplinary approach for its understanding and development. The core study provided important information about the porosity, permeability and mineralogical composition of the rocks, which is critical for assessing their reservoir properties and hydrocarbon recovery efficiency. Hydrochemical analysis of water revealed high mineralization and hardness of the

water, which requires special attention when planning water treatment and disposal systems. Petrographic and mineralogical studies of rocks have provided detailed data on their textural and structural features and processes of secondary transformation, which contributes to a deeper understanding of the conditions of rock formation and their properties. Analysis of reservoir fluids, in turn, highlighted the compositional and thermodynamic conditions of reservoir oil and gas, which are key to developing and maintaining production. In general, the results of studies of the “X” oilfield provide a valuable database for further geological modeling, development and optimization of hydrocarbon production methods. This data not only facilitates efficient field development, but also makes a significant contribution to scientific knowledge about such geological objects, allowing for improved methods of exploration and exploitation of oil and gas resources.

3. METHODOLOGY

3.1. Bulk foam stability test

The foam stability test was dedicated to screening foam formulations that could be applied to further experiments. Due to connate water hardness issues and the incompatibility of multivalent ions with many surfactants, it is assumed that preconditioning of the reservoir is needed and would be conducted during the late stages of water flooding. The experiment evaluates how the different concentrations of NaCl, bio-surfactant, and nanoparticles in distilled water affect foam stability. Nitrogen acts as a gas for foam generation. The following equipment is used during the experiment: a magnetic stirring device, a homogenizer (Figure 17), a 500 ml volumetric flask, a highly permeable diffuser as a foam generator, and a digital camera.

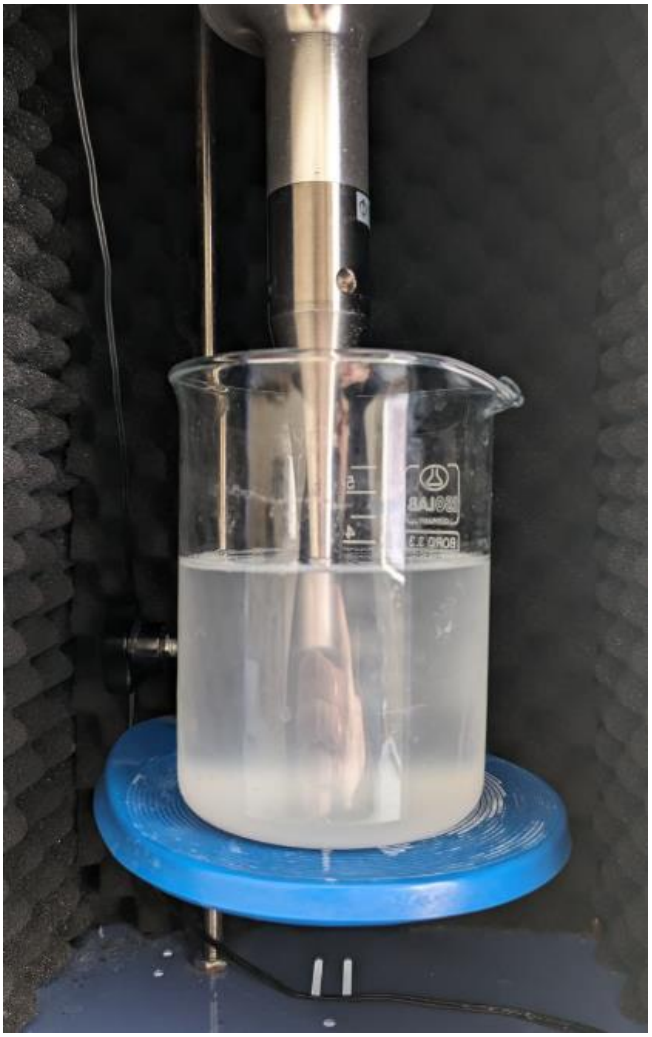

Figure 17. Photo of homogenizer application to prepare nanoparticle (np) solutions

The foam half-life time experiment design consists of two parts: preparation of solutions and generation of the foam, followed by subsequent documentation of the pattern of its degradation (Figure 18). The solution is prepared by sequentially dissolving NaCl, bio-surfactant, and nanoparticles in distilled water. Each stage of preparation is accompanied by stirring the composition using a magnetic stirrer for half an hour at a speed of 250 rpm. Due to the difficulty of dispersing nanoparticles in a solution, it is necessary to leave the solution for 15 minutes in an ultrasonic homogenizer, resulting in increased transparency of the solution. When the solution is ready, it is placed in a volumetric flask with a diffuser lowered inside; gas is supplied through the diffuser which, passing through the prepared solution, forms a column of foam (Figure 19).

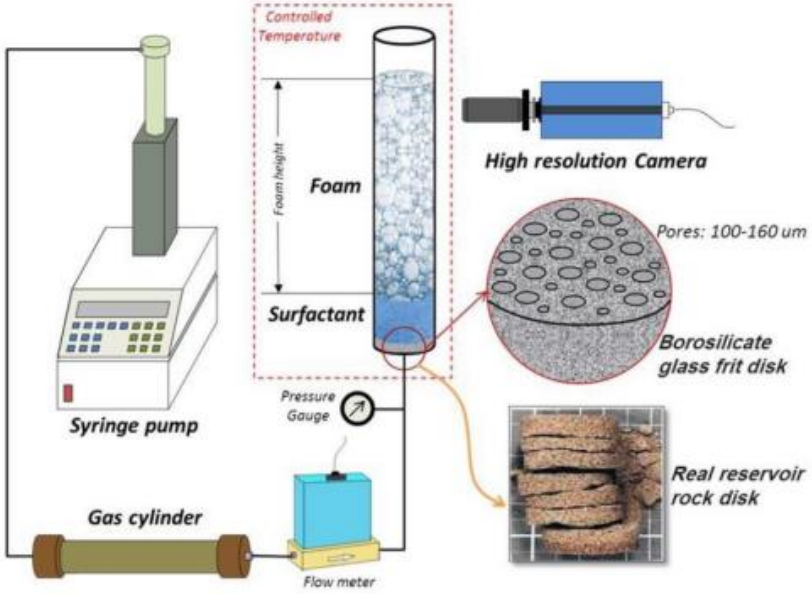

Figure 18. Foam stability test setup [40]

After the column reached a volume of 500 ml, the nitrogen supply was stopped, and the process of foam degradation was monitored. The pattern of foam degradation is captured by the camera, with special attention paid to the behavior of the foam when reaching the 400 and 300 ml levels (Figure 20).

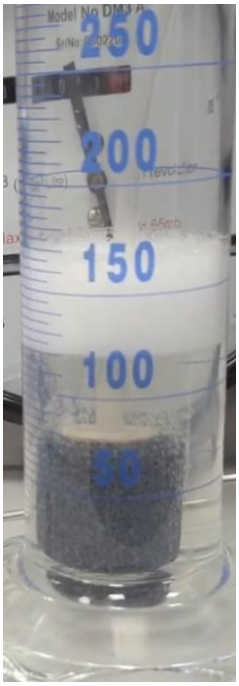

Figure 19. Foam generation through using diffuser

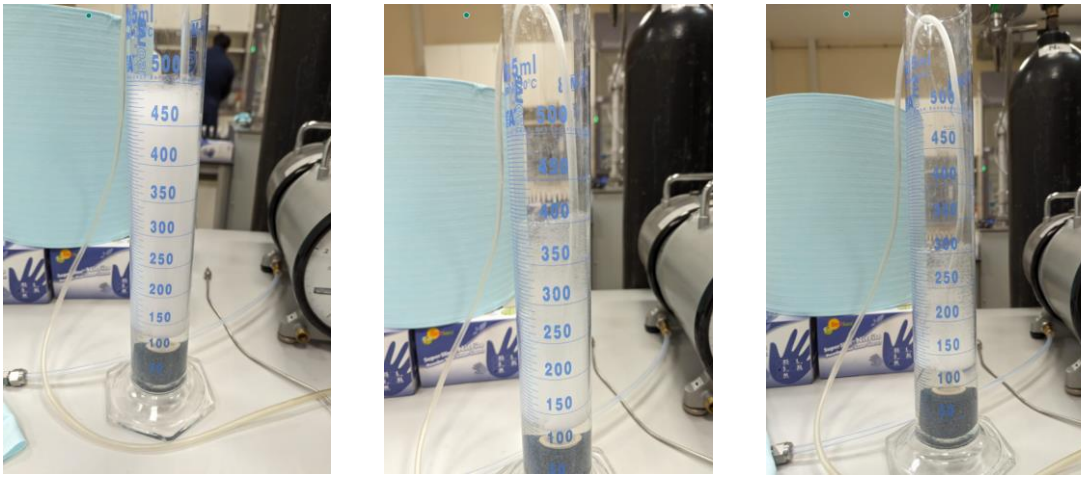

a) b) c)

Figure 20. Experiment flow of foam stability test:
a) The foam column at the start of experiment, b) The foam column during the experiment, c) The foam column at the end of the experiment

The effects of increasing salinity and nanoparticle concentration on foam stability were examined. Two expected effects were considered: the detrimental effect of increasing salt concentration and the benign effect of increasing nanoparticle concentration on foam stability. To investigate how different concentrations of surfactant and sodium chloride affect foam

stability, the experiments were repeated with different proportions of surfactant and salt. Table 3 shows the combinations examined.

Table 3. Bio-terge surfactant and salinity variation for foam test stability

BIO-TERGE surfactant, %
0,1
0,25
0,5
0,75

a)

NaCl %
0,005
0,25
0,5
1
2,5
3,5

b)

The graphs allow us to determine the most effective solution of the foam for conducting further experiments of core-flooding.

3.2. Core description

The second type of experiment conducted is core flooding. The purpose of the core flooding experiment is to identify the efficacy of foam generation and propagation in porous media and how foam interacts with the residual oil from prior displacement processes. For the core flooding experiment, we use a solution for foam generation, the composition of which was determined from half-life tests conducted previously. One-inch diameter core samples collected from the "X" oilfield, by core drilling technique, are shown in Figure 21.

Figure 21. Oilfield "X" reservoir core plugs used in coreflood experiments.

Table 4. Core sample parameters

	diameter	length	Volume	Dry weight	Wet weight	Water weight	Void volume	Porosity	Permeability	Depth
	mm	mm	mm^3	g	g	g	mm^3	fraction	mD	m
Indiana	38.1	73.2	83400	190.1	201.7	11.63	11630	0.14	24	
Berea	38.1	73.8	83900.	181	195.5	14.42	14420	0.17	195.3	
"X-15"	37.6	52.7	58500	131.9	140	8.14	8140	0.08	0.15	3178.93
"X-13"	37.6	53.1	59000	134.6	139.3	4.74	4740	0.14	0.2	3178.36
"X-10"	37.7	54.0	60200	135.5	143.6	8.03	8030	0.13	0.45	3177.37

For visual coloration of dodecane, an insignificant amount of heavy oil was added. Dodecane properties are given in Table 5.

Table 5. Dodecane physical and chemical properties [27] [28][29]

Chemical Formula	$C_{12}H_{26}$
Molecular Weight	170.34 g/mol
Appearance	Colorless liquid with a mild aliphatic hydrocarbon odor
Melting Point	Approximately −10.0 to −9.3 °C (14.1 to 15.2 °F)
Boiling Point	Approximately 214 to 218 °C (417 to 424 °F)
Density at 20 °C	0.7495 g/mL
Viscosity at 25 °C	1.34 mPa·s
Vapor Pressure at 25 °C	18 Pa
Flash Point	71 °C (160 °F)
Autoignition Temperature	205 °C (401 °F)
Refractive Index at 20 °C	1.421
Water Solubility	Less than 1 mg/mL at 25 °C
Odor	Gasoline-like to odorless
Critical Temperature	Approximately 385 °C
Critical Pressure	Approximately 18 bars

3.3. Core flooding experiment

A core saturator is needed to prepare the core for further flooding. The core flooding experiment is conducted using the "Core Flooding System (CFS-350)" by Vinci Technologies. The apparatus is presented in the FOAM EVAL-HPHT Foam Analyzer setup, which allows for the measurement of parameters such as gas flow rate, liquid flow rate, and volume injected in real time, which is needed to obtain a reliable evaluation of efficiency. The experimental procedure begins with the preparation of the core sample, which is essential for subsequent flooding experiments. First, the core must be placed in a core saturator filled with 1% NaCl brine under vacuum conditions. This step ensures the complete saturation of the core sample. As part of the apparatus setup, the core sample is placed in the core holder, and to avoid channeling or flooding the fluid side of the core, the confining pressure is set at a value of 300 PSI. The next step is to charge the accumulator with oil. When the equipment is completely assembled, the flooding operation should be started. The flooding starts with oil injection. The oil is injected until no more brine is produced. At the end of the oil injection, the rock sample is in conditions that maximally replicate the initial conditions of the reservoir with initial oil and connate water saturation. As foam flooding is a tertiary recovery method that is applied at the very end, conventional flooding techniques, such as water flooding and gas flooding, should be conducted first. The gas and water flooding designs differ from initial oil flooding only by the liquid injected into the core-gas and water, respectively. The influence of capillary pressure end effects in the flow-based approach was studied by conducting brine injection at different flow rates. Higher flow rates reduce the capillary effect and help in the evaluation of displacement efficiency under viscous flow conditions, whereas lower flow rates emulate capillary-dominated conditions, resulting in more selective oil displacement. After conventional water flooding, the core will be in the condition of residual oil and high water cut, which most accurately reflects the current condition of the oil reservoir of the "X" oilfield. After water flooding, gas flooding proceeds to the point of residual oil to gas flooding. For conducting the foam flooding experiment, simultaneous injection of nitrogen and foam solution is needed (Figure 22).

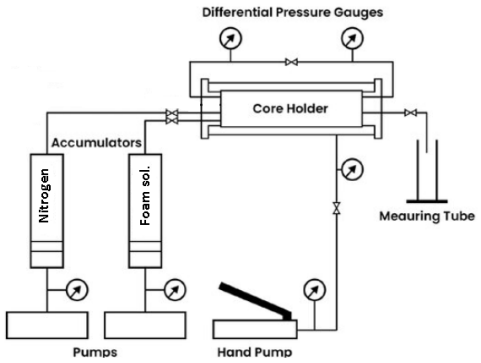

Figure 22. Schematic of the SRP 350 core flooding apparatus setup for foam flooding by Vinci Technologies [56]

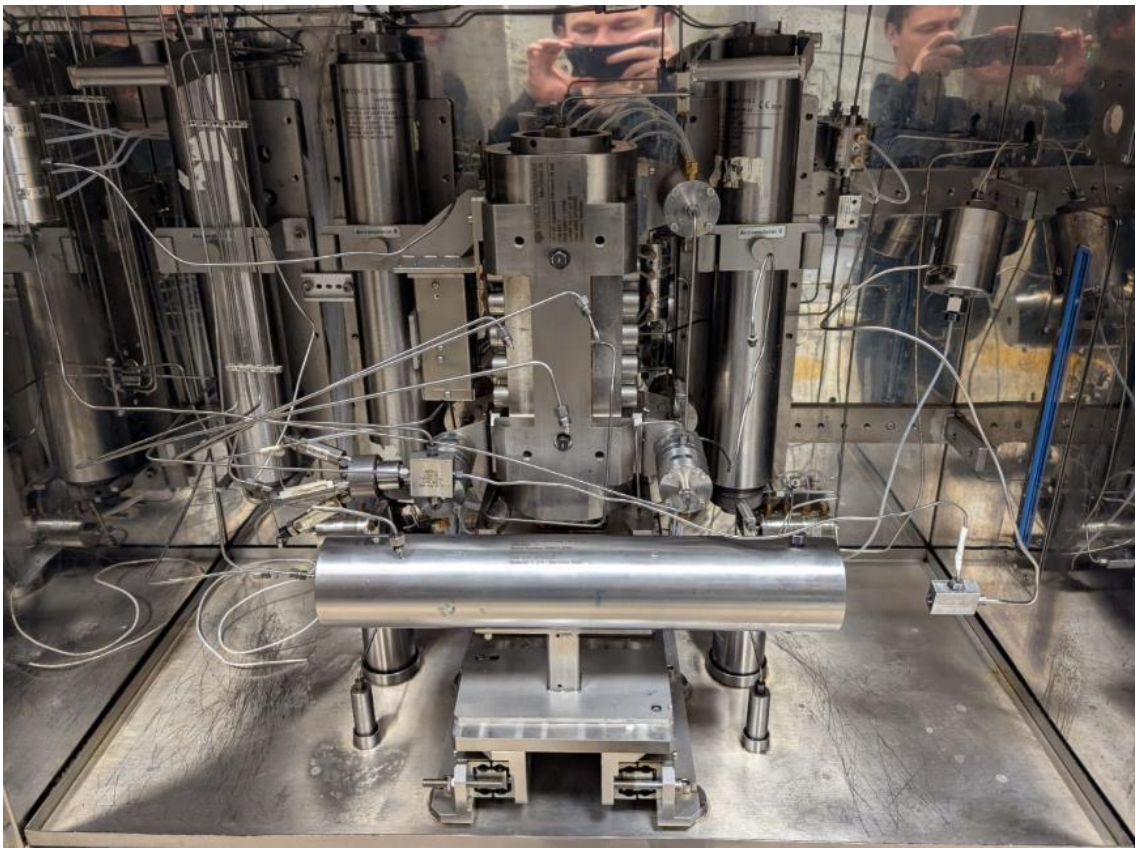

Figure 23. Photo of core flooding experimental setup

Additionally, to investigate the lamella hardness effect of foam on the recovery factor, foam flooding is repeated but with the addition of 0.1 % nanoparticles into the foam solution. The flooding is conducted until the oil production stops. During the experiment, the data is collected in real-time automatically by Vinci Technologies software with the possibility of subsequent data export. For the data analysis, the charts of pressure difference vs. pore volume injected and

recovery factor are built in one plot. Such a plot is created for each flooding step, i.e., for water, gas, foam, and foam with nanoparticle addition. From the charts, it is possible to evaluate the pressure difference response to the production of additional oil during the continuous flooding that is necessary for the evaluation of flooding process efficiency. After core flooding with N_2 application is finished, the core is carefully cleaned by the Soxhlet extraction method with the application of toluene solvent (Figure 24) to prepare the core for the duplicate experimental suite, but with CO_2 gas instead of N_2.

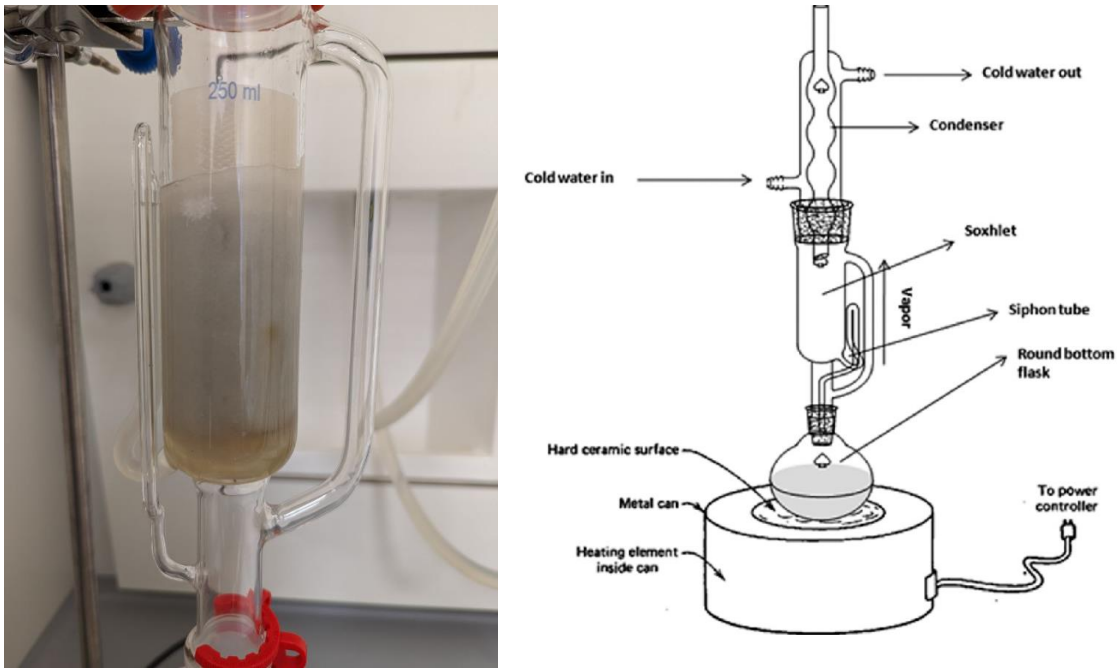

a) b)

Figure 24. Soxhlet extractor
a) Photo of extraction process b) Cleaning setup[54]

3.4. Experimental analysis

From flooding experiment data, graphs were plotted of the recovery factor and pressure difference from the flooding experiment as a function of pore volumes injected. Additionally, plots of recovery factor against apparent viscosity with increasing pore volume injected were generated. The estimated apparent viscosity (since the flooding was modeled a single-phase flow), was computed by means of Darcy's law.

$$\mu_{app} = \frac{k * A * \Delta P}{14700 * Q_t * L}$$

Where:

$\mu_{app}\ (cP) - apparent\ viscosity$
$\Delta P\ (psig) - pressure\ drop$
$Q_t\ (^{cc}/_{s}) - injection\ flow\ rate$
$L\ (cm) - core\ lenght$
$A\ (cm^2) - core\ cross\ section\ area$
$k\ (mD) - permeablity$

Darcy's law is used in that it is a reliable method to describe fluid flow through porous media and to obtain an understanding of the effect of viscosity on flow dynamics during the displacement process. In such an approach, the apparent viscosity captures overall mobility, which is a combination of fluid viscosity and saturation-dependent relative permeability. This enables comparison of performance across cores of vastly different permeability that would be difficult to understand in terms of pressure drop.

4. RESULTS AND DISSCUSSION

4.1. Foam stability test

Figure 25 illustrates the foam half-life time for the various salinity and AOS surfactant concentrations. From the figure, it is obvious that the half-life time differs only at the very low salinity until 1 %, and with increasing salinity, half-life time variation shrinks and is drastically reduced. From the figure could be observed that the dependence of foam half-life time is not directly dependent on surfactant concentration for concentrations above 0.1 %. The maximum foam life time corresponds to a surfactant concentration of 0.25 %, while the concentration of 0.75 % represents a typical value of half-life time. However, at the salinity of 1 %, the trend is reverses with 0.75 % surfactant concentration giving the best results. This phenomenon can be attributed to the negligible dependence of foam stability on surfactants concentration above the critical micelle concentration (CMC) of 0.3 g/L [55]. Since 1 % salinity is selected as representative of reservoir brine, the typical result using less chemical is chosen for core flood experiments. Core flood experiments using foaming formulations were, hence, conducted with 0.25 % surfactant and 1 % brine.

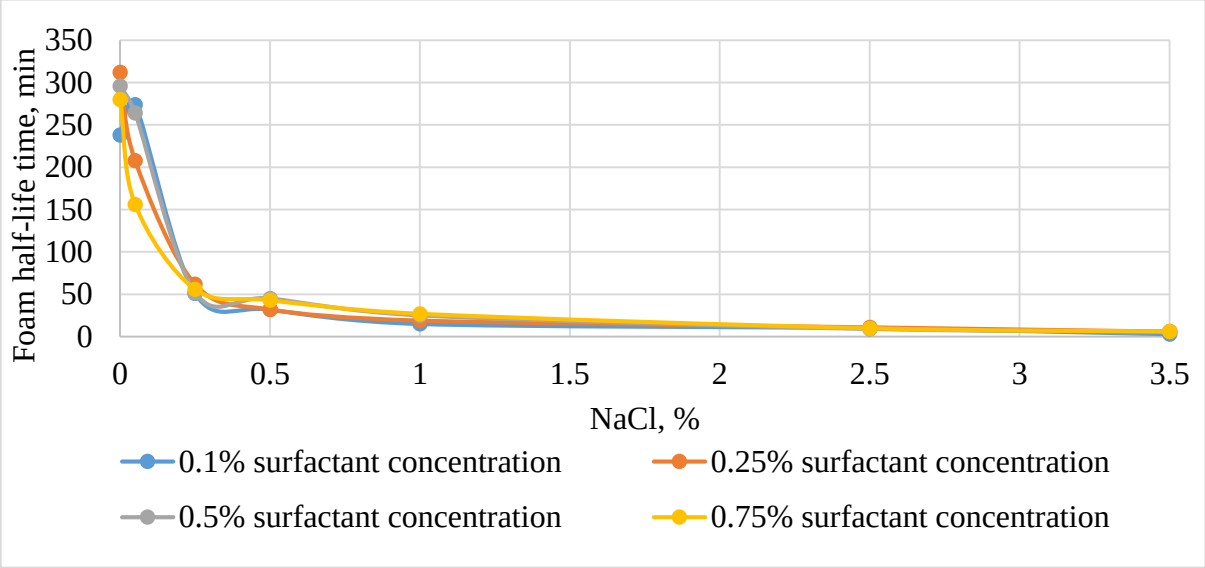

Figure 25. Foam stability test results

The foam that was just generated has bubbles in the range of 0.5 mm in diameter, while at the final stage of the experiment, the bubbles could reach 10 mm in diameter (Figure 20).

To better understand the difference between N_2 and CO_2-generated foam stability at atmospheric conditions, results from a similar experiment conducted by Bello et al. (2022) with CO_2 generated foam are presented as Figure 26.

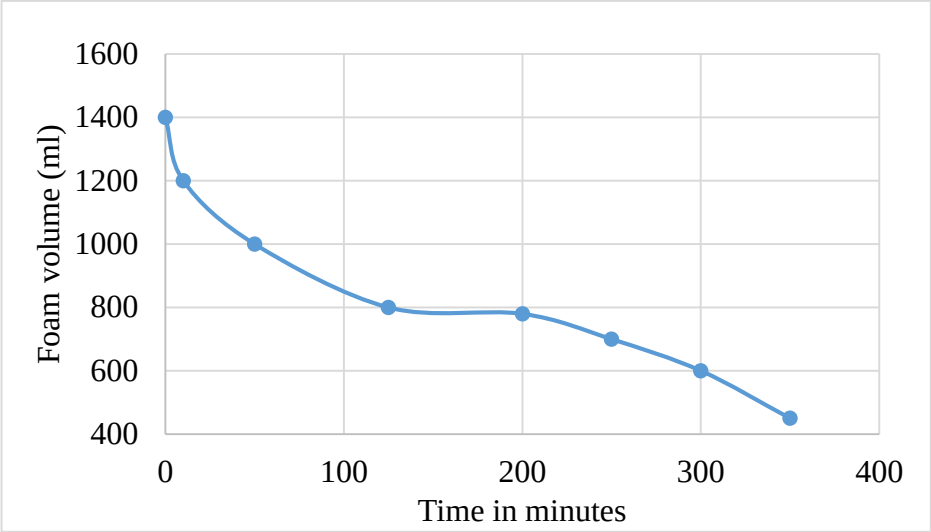

Figure 26. CO_2 bulk foam generated by 0.1 % BIO-TERGE surfactant and 0.5 % of silica nanoparticles in 1 % NaCl [41]

By comparing the data, it is feasible to determine that the half-life of nitrogen foam containing 0.1 % silica nanoparticles and 0.1 % BIO-TERGE surfactant in 1 % NaCl was 16.6 % longer than that of CO_2 foam using the same chemical solution.

4.2. Oilfield "X" core sample flooding results

4.2.1. *"X-10" Core flooding experiment results*

Figure 33 illustrate how the apparent viscosity and recovery factor change with the pore volume (PV) injected and the pressure difference required to flow at the chosen constant rate. The flooding scheme started core preparation to achieve the starting condition of initial oil saturation at immobile brine saturation. This is followed by displacement experiments starting with brine injection, followed by gas injection, foam injection, and final foam flooding with nanoparticle addition. Waterflooding was conducted in order to produce residual oil condition as the starting point for any enhanced oil recovery methodology, as the brine injection is the most conventional secondary recovery technique that is applied in the majority of the field. Reservoir brine was represented by

a 1 % NaCl solution with the assumption that reservoir preconditioning was necessary to suppress divalent ion interactions with added foam stabilizers. To investigate how the viscous forces, affect the flooding process and eliminate capillary end effects, the brine flooding was conducted in 3 stages: 1 cc/min, 2 cc/min, and 3 cc/min injection flow rate. From the figure, the effect flow rate on the pressure drop could be clearly obtained. Each step of the flow rate increase is accompanied by an increasing pressure difference response, accompanied by additional recovery and corresponding saturation-dependent relative permeability changes. As observed in Figure 30, the total recovery factor (RF) achieved after brine injection was 15.36 % after 15.5PV was injected. By this step of injection, the reservoir is in the terminal condition of secondary recovery which is needed for further recovery techniques and comparison of EOR flooding techniques.

To examine the foam flooding effect, it is needed to treat the foam flooding as an independent technique to separate foam flooding recovery mechanisms from those of gas flooding. Thus, gas flooding was performed after waterflooding as a natural injection sequence prior to a decision to initiate foam flooding to resolve conformance issues in gas flooding. Thus, nitrogen gas flooding was conducted after reaching waterflood residual oil saturation. Figure 30 shows that with a 1 cc/min gas flow rate, a recovery efficiency of 29.3 % was achieved in nitrogen gas flooding. From the gas flooding pressure drop response, the moment of the gas breakthrough could be observed. After a cumulative effect of 30 PV of fluid injection, the curve acquired a plateau trend, followed by stabilization at a significantly lower pressure drop than waterflooding, which is explained by lower resistance to gas flow through a porous media. The graph reached a plateau in recovery factor coincident with gas breakthrough. With an established residual oil to gas flooding terminal condition, the results of the subsequent foam flooding can be assessed independently.

The foam flooding without nanoparticles increased oil production from 29.3 % to 35 %. The foam was generated by simultaneous injection of 0.25 % surfactant solution and nitrogen. The flow rate was established as 0.6 cc/min for foam solution injection and 0.4 cc/min for N_2 gas injection, with the total flow rate fixed at 1 cc/min. This gas fractional flow was chosen based upon the observed stability of foam exiting the core flood in

screening tests (see Figure 30). In the plateau phase for recovery, the apparent viscosity reached 6.5 cP. With the expectation of higher-pressure difference responses with increasing flow rate and the challenges of foam stability control, the flooding was conducted using only one flow rate.

Figure 27. Observed process, of foam pushing out the out, in transparent tube installed on outlet line

The effect of foam lamella integrity on residual oil production was investigated by adding silica nanoparticles into the solution. For a fair comparison, the flooding design remains the same as foam flooding without nanoparticles. From the flooding diagram can be observed that 0.1 % nanoparticles in the foam solution allowed production of an additional 3.3 % of oil with a total oil produced value of 38.3 %. The apparent viscosity at the steady flow reached 8.5 cP, which is 23 % higher than in foam injection without nanoparticles. The character of production collected in outlet line changed significantly with the addition of nanoparticles to the foam flooding formulation (Figure 28). From the pressure response, it can be inferred that adding nanoparticles into the foam solution allows for an increase in lamella resilience that in turn leads to significantly higher propagation pressure to support a fixed injection rate. The results of nanoparticle application demonstrate a positive effect on the production of residual oil, but only if reservoir displacement processes can support such a pressure drop.

a)

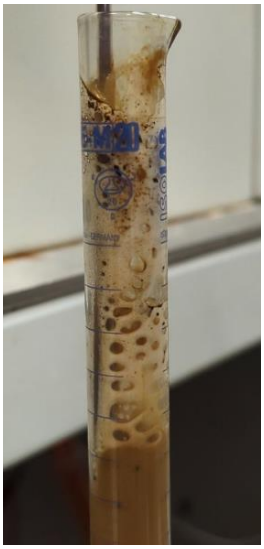

b)

Figure 28 Comparison of foam texture of nitrogen generated foam (a) and CO_2 generated foam (b)

To examine the distinctions between the application of CO_2 and N_2 foam, core sample "X-10" was cleaned using the Soxhlet extraction method (Figure 29) and the injection sequence was repeated with CO_2 instead of N_2.

a)

b)

Figure 29. Indiana core sample (a) before and (b) after cleaning

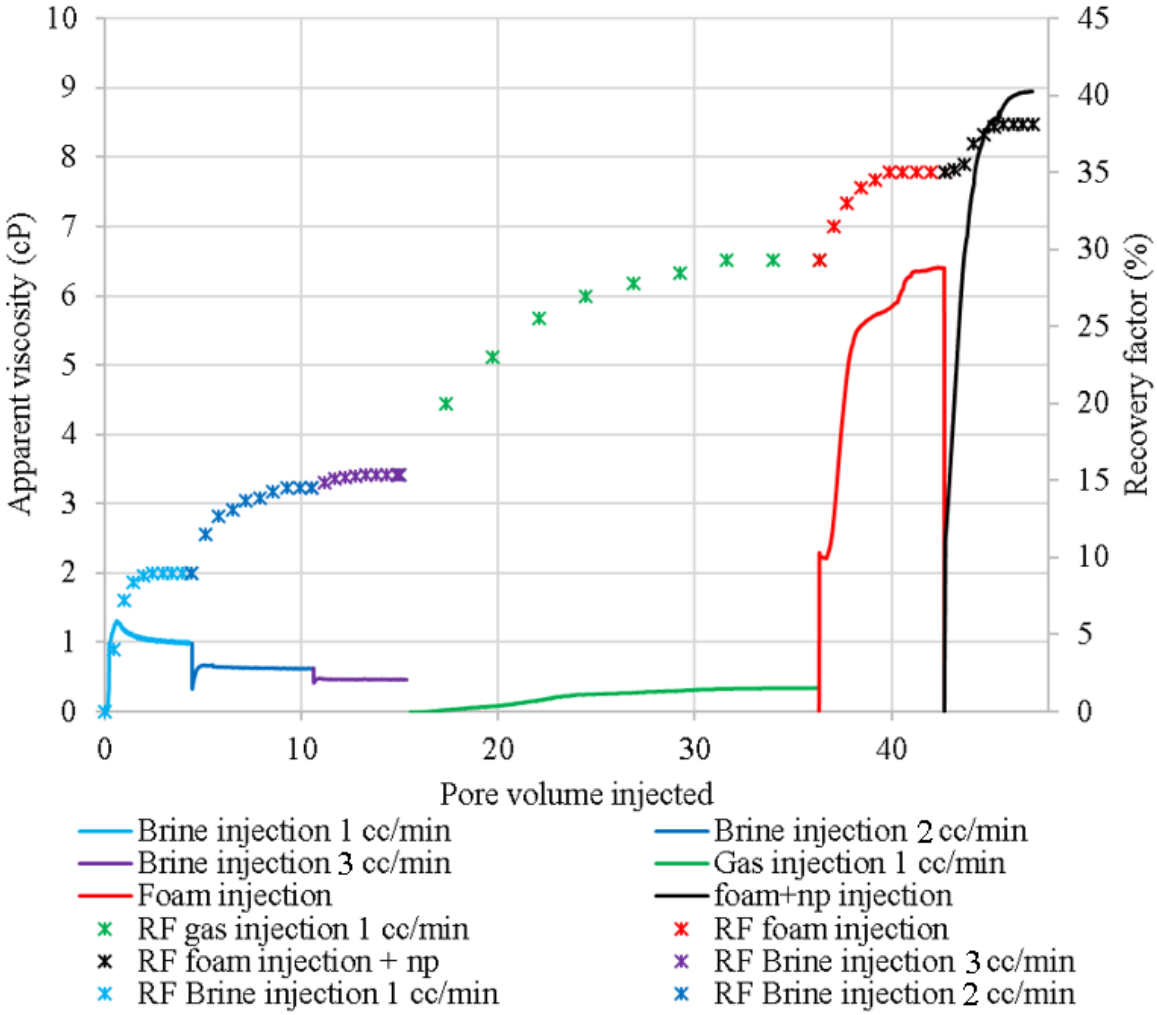

Figure 30. N_2 application "X-10" core flooding experiment results apparent viscosity and RF vs PV

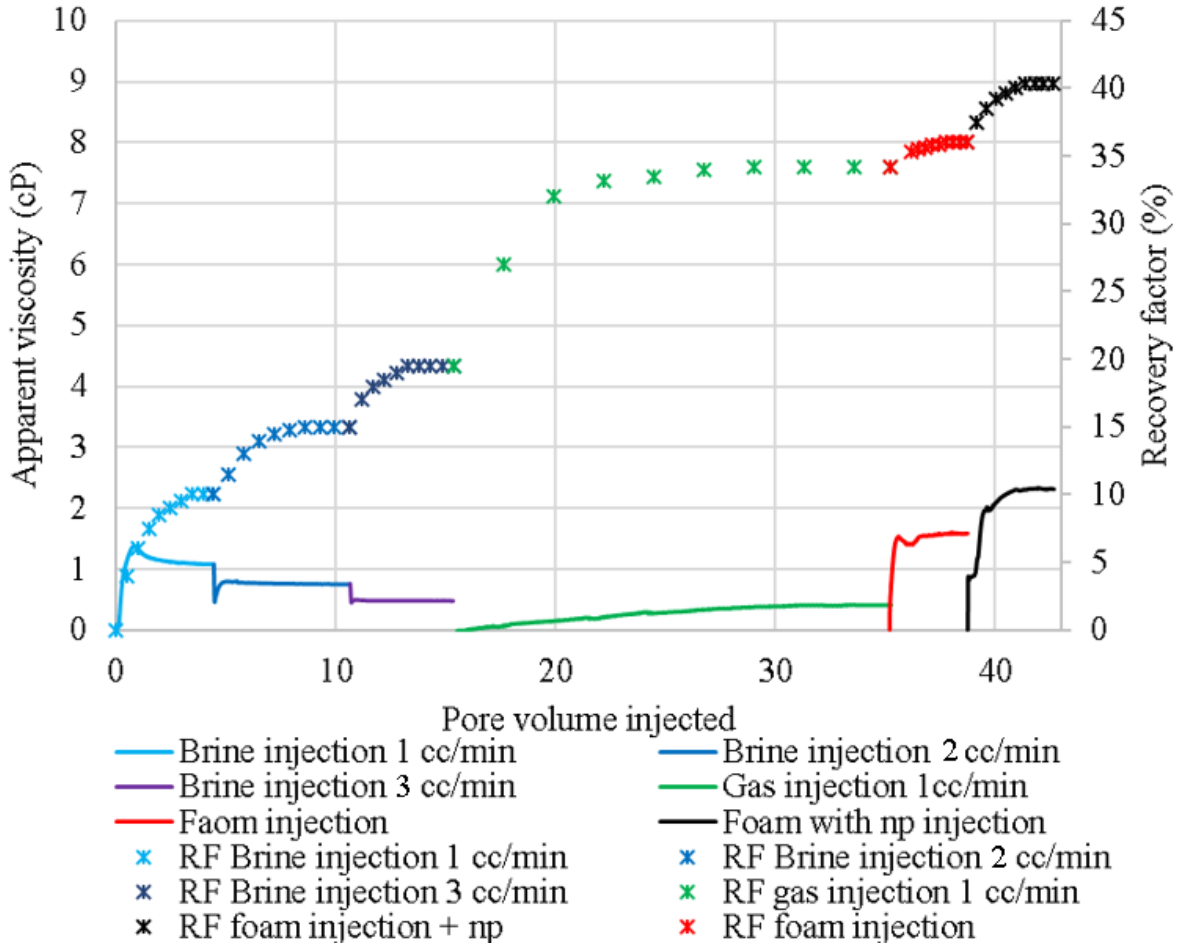

Figure 31. CO_2 application "X-10" core flooding experiment results, apparent viscosity and RF vs PV

Table 6. "X-10" core flooding recovery factor increment comparison table

	RF	
	N_2	CO_2
Water flooding 1cc/min	9	10.1
Increment	*+5.5*	*+4.9*
Water flooding 2cc/min	14.5	15
Increment	*+0.86*	*+4.5*
Water flooding 3cc/min	15.36	19.5
Increment	*+13.94*	*+14.7*
Gas flooding 1c/min	29.3	34.2
Increment	*+5.7*	*+1.8*
Foam flooding 1cc/min	35	36
Increment	*+3.3*	*+4.4*
Foam np flooding 1cc/min	38.3	40.4

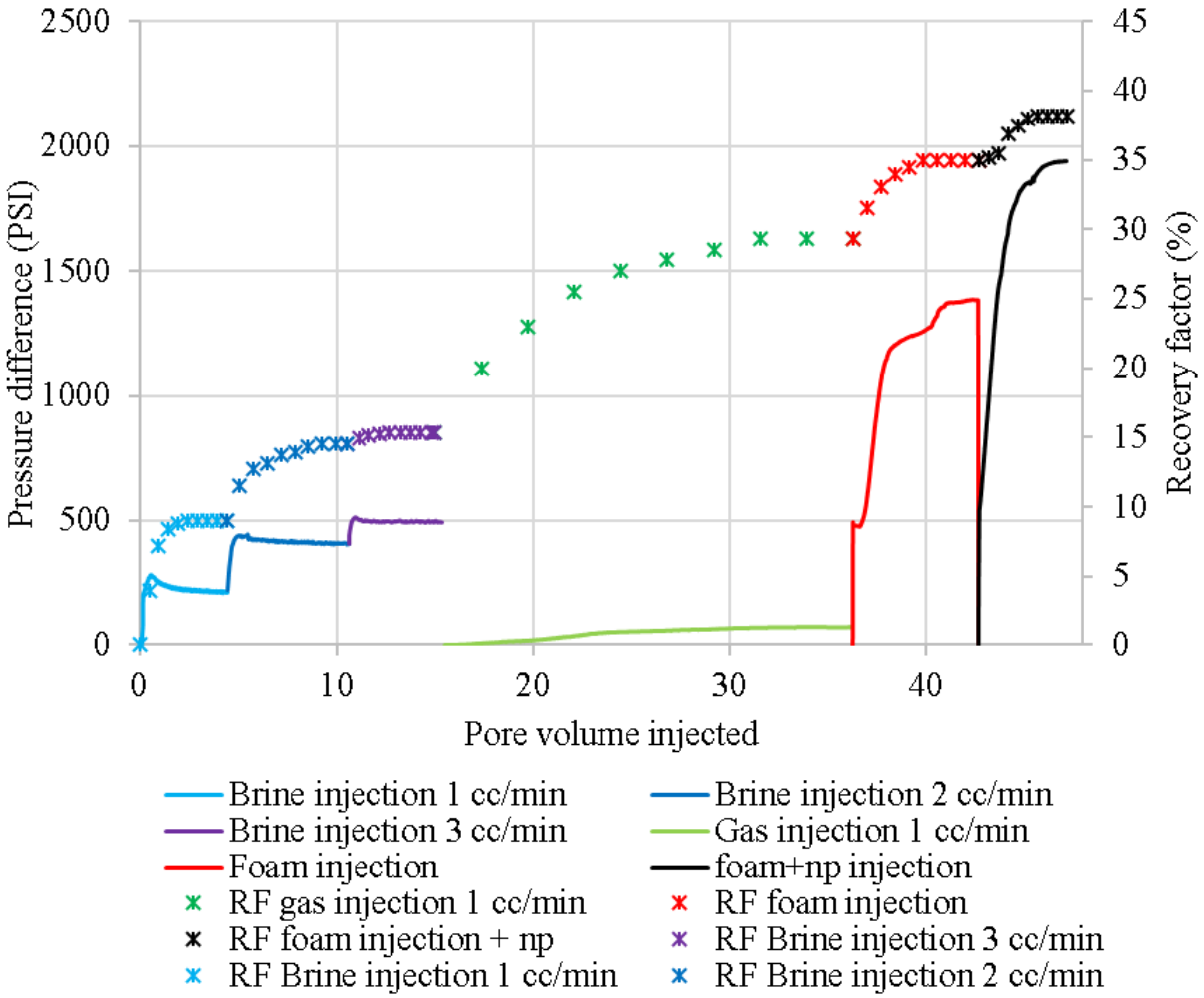

Figure 32. N_2 application "X-10" core flooding experiment results differential pressure and RF vs PV

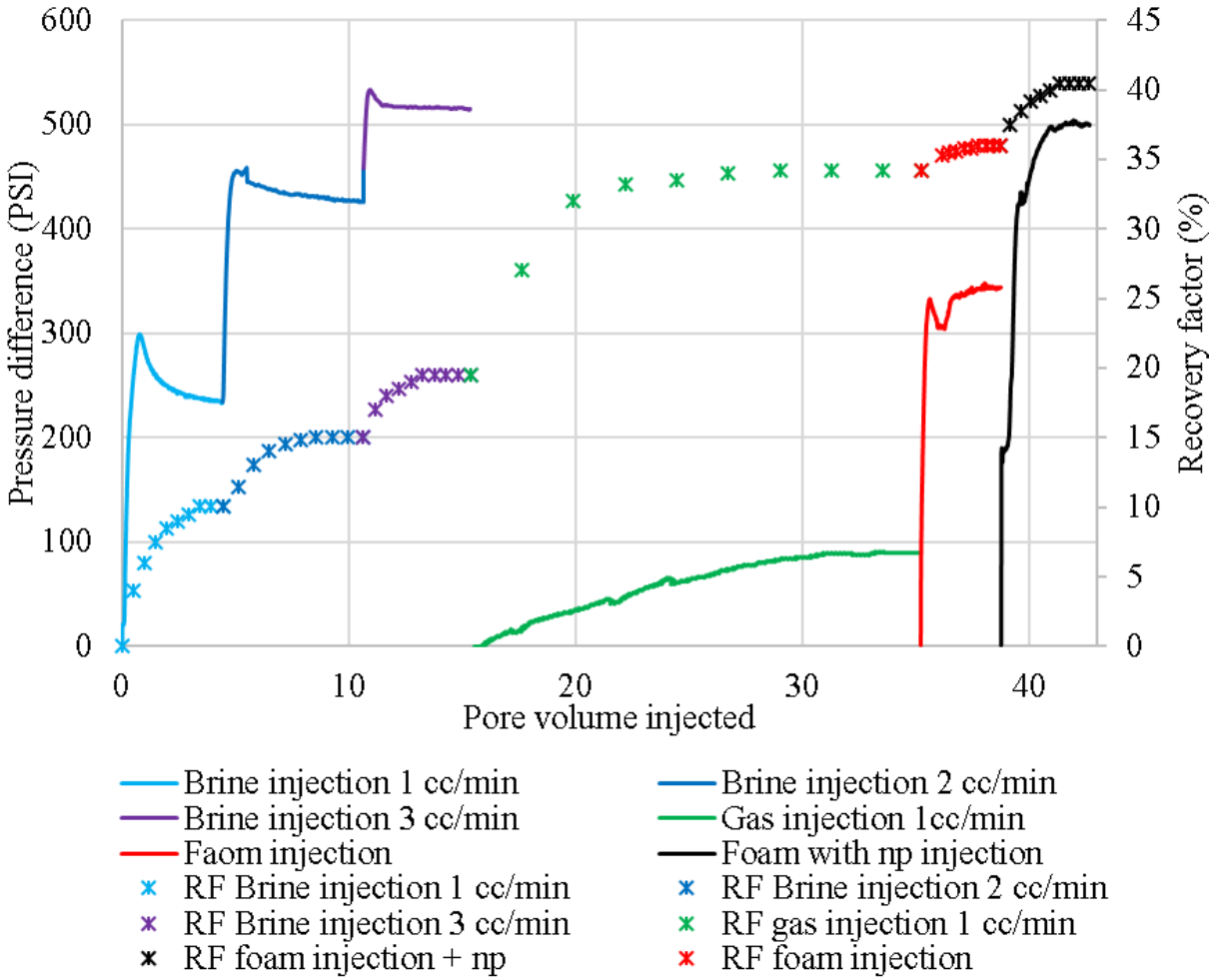

Figure 33. CO_2 application "X-10" core flooding experiment results differential pressure and RF vs PV

The shift from nitrogen to carbon dioxide as the gaseous phase in the core flood experiment (Figure 30) introduced significant alterations in the observed pressure and recovery dynamics, reflecting the distinct properties of CO_2. Notably, CO_2 injection alone yielded higher incremental oil recovery, in stark contrast to the moderate increase observed with nitrogen gas. This difference may be attributed to several factors, including: (1) the higher solubility of CO_2 in oil, leading to swelling and viscosity reduction but also potential trapping of CO_2 within the pore space; (2) the potential for CO_2 to alter the interfacial tension between oil and water, affecting capillary forces and displacement efficiency; and (3) the potential for CO_2 adsorption onto the rock surface, altering wettability. The lower increase in the pressure drop during CO_2 foam injection, coupled with the "bumpy" pressure curve, indicates differences in foam stability compared to the nitrogen foam system. In particular, CO_2 may diffuse through lamellae quickly and also has a tendency to change the wettability as compared to N_2 foam which contributes to

the reduced foam quality. The nanoparticles have a higher proportional impact on oil recovery, further highlighting the complex interplay of fluid properties, interfacial phenomena, and pore-scale interactions in CO_2-based enhanced oil recovery. Ultimately, the success of CO_2 foam for enhanced oil recovery is more complex. The change in nanoparticles can also be higher. However, CO_2 foam is generally less stable.

4.2.2. *"X-13" Core flooding experiment results*

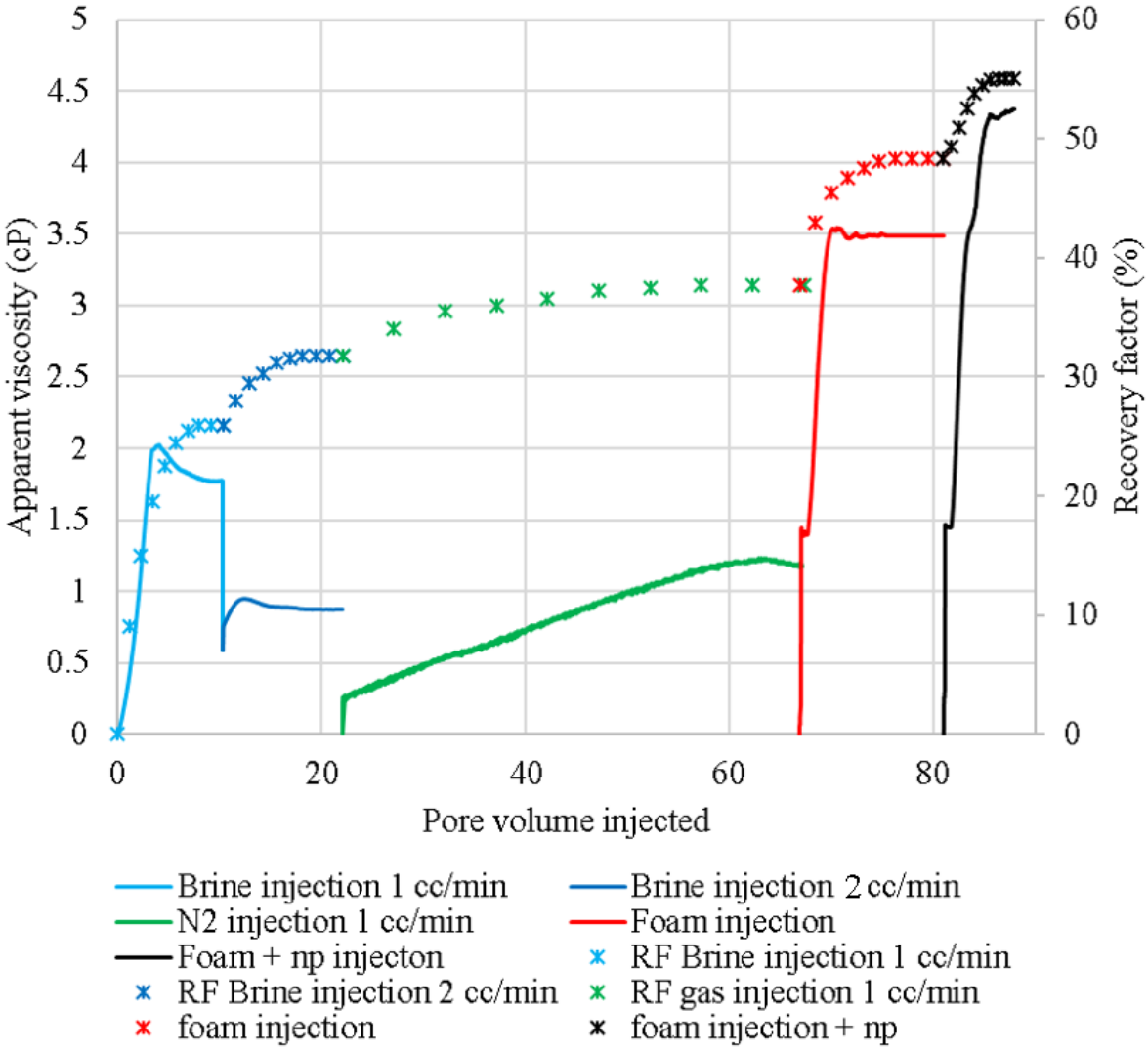

Figure 34. N_2 application "X-13" core flooding experiment results apparent viscosity RF vs PV

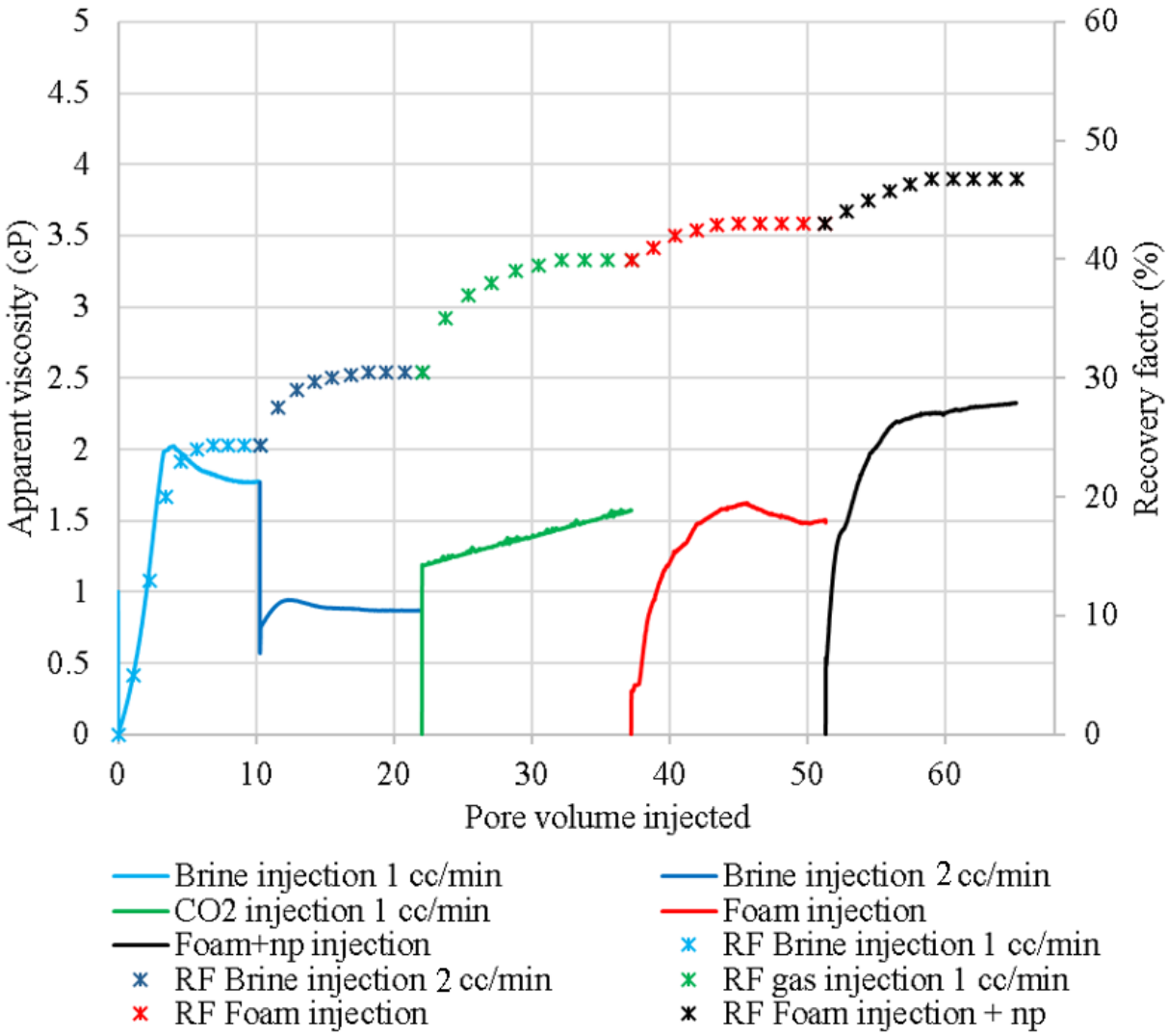

Figure 35. CO_2 application "X-13" core flooding experiment results apparent viscosity and RF vs PV

Table 7. "X-13" core flooding recovery factor increment comparison table

	RF	
	N_2	CO_2
Water flooding 1cc/min	26	24.32
Increment	*+5.8*	*+6.18*
Water flooding 2cc/min	31.8	30.5
Increment	*+5.9*	*+9.4*
Gas flooding 1c/min	37.7	39.9
Increment	*+10.6*	*+3.1*
Foam flooding 1cc/min	48.3	43
Increment	*+6.8*	*+3.8*
Foam np flooding 1cc/min	55.1	46.8

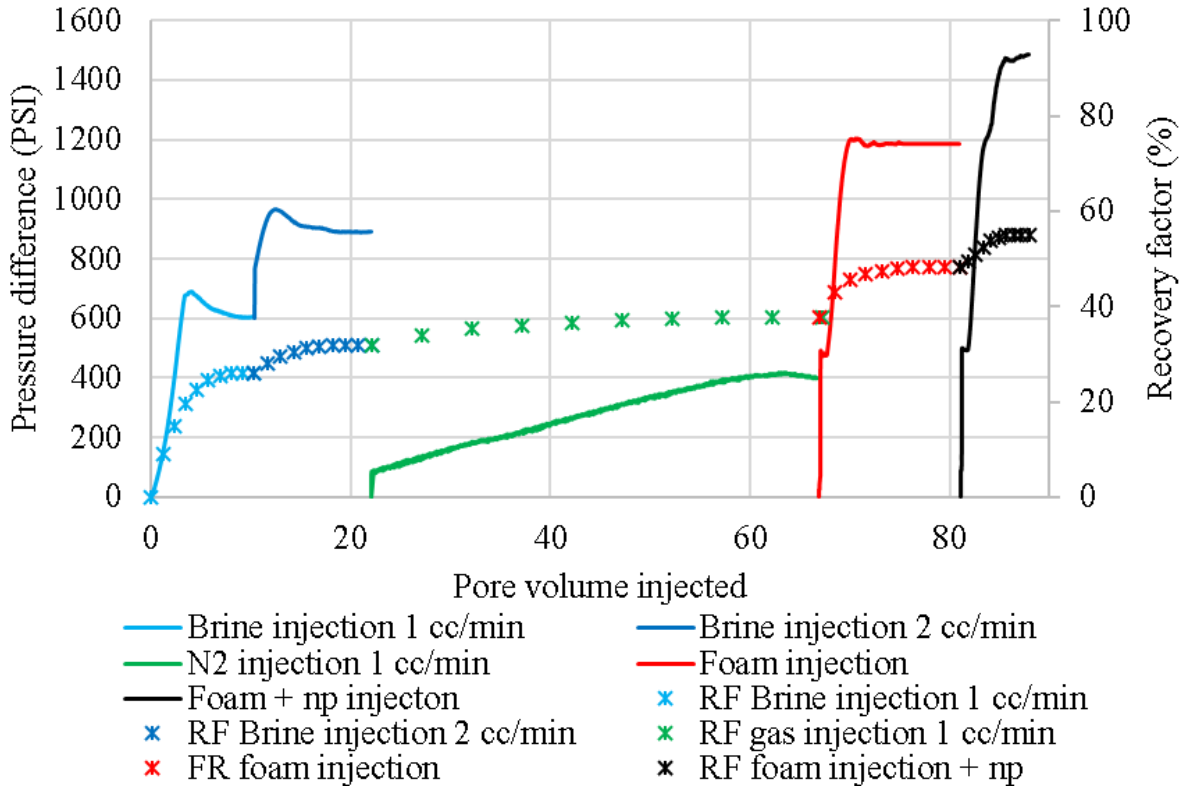

Figure 36. N_2 application "X-13" core flooding experiment results dP, RF vs PV

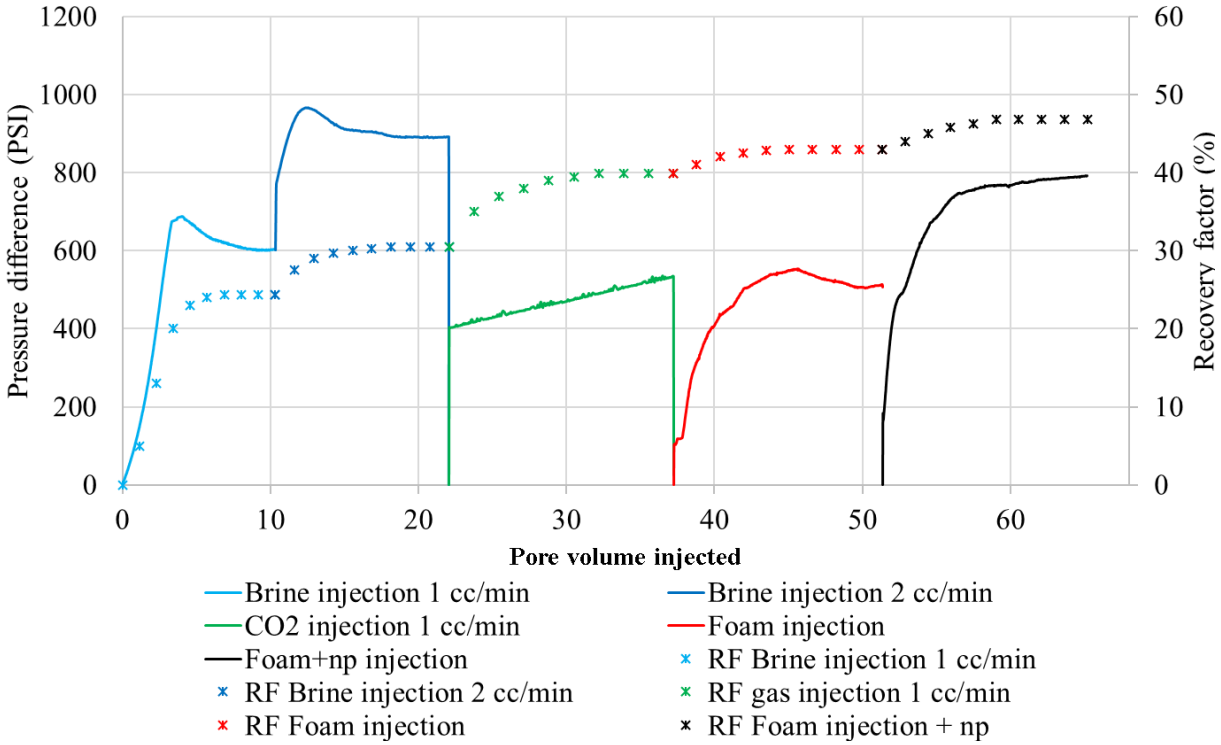

Figure 37. CO2 application "X-13" core flooding experiment results dP, RF vs PV

4.3. Outcrop core samples flooding results

4.3.1. *Berea core sample flooding result*

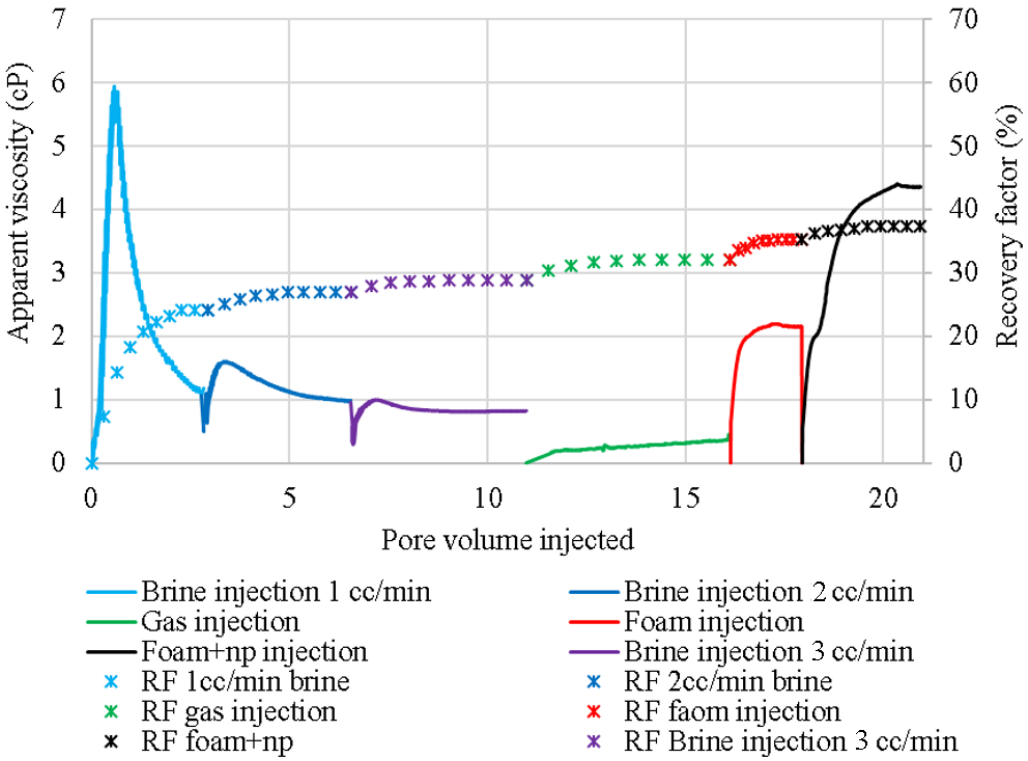

Figure 38. N_2 application Berea core flooding experiment results apparent viscosity and RF vs PV

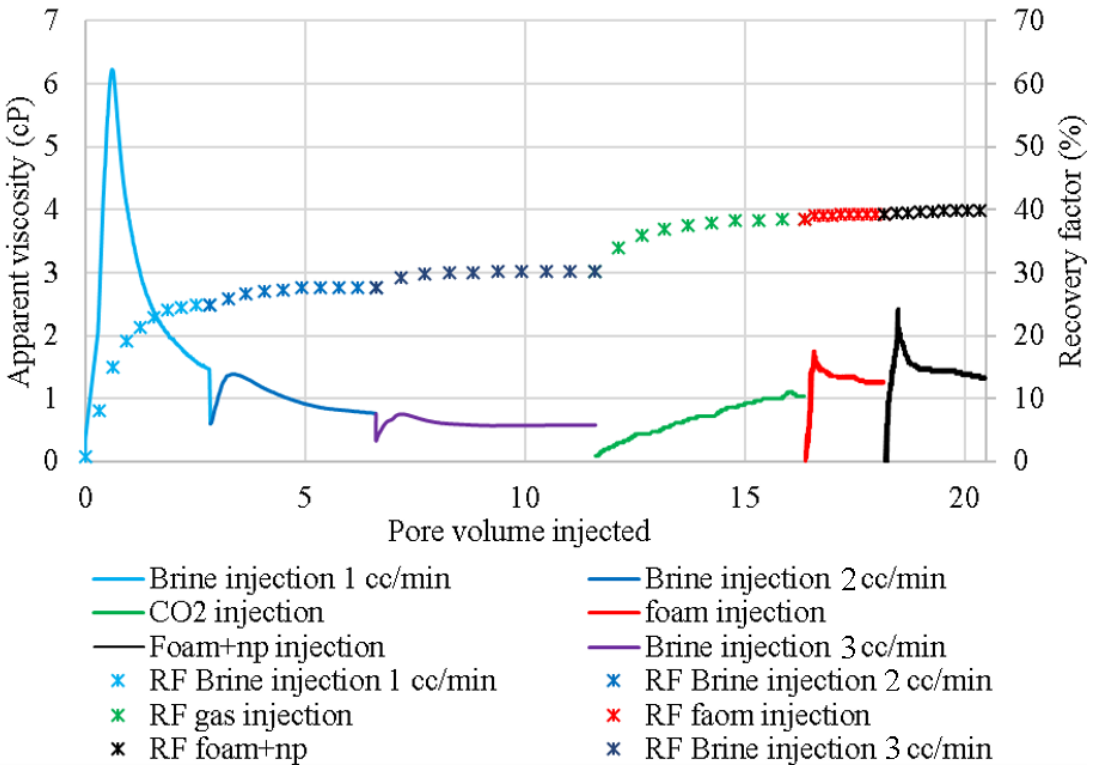

Figure 39. CO_2 application Berea core flooding experiment results apparent viscosity and RF vs PV

Table 8. CO_2 and N_2 foam Berea core sample flooding comparison

	RF	
	N_2	CO_2
Water flooding 1cc/min	24.13	24.88
Increment	*+2.77*	*+2.77*
Water flooding 2cc/min	26.9	27.65
Increment	*+1.9*	*+2.5*
Water flooding 3cc/min	28.8	30.15
Increment	*+3.32*	*+8.35*
Gas flooding 1c/min	32.12	38.5
Increment	*+3.08*	*+0.7*
Foam flooding 1cc/min	35.2	39.2
Increment	*+2.1*	*+0.9*
Foam np flooding 1cc/min	37.3	40.1

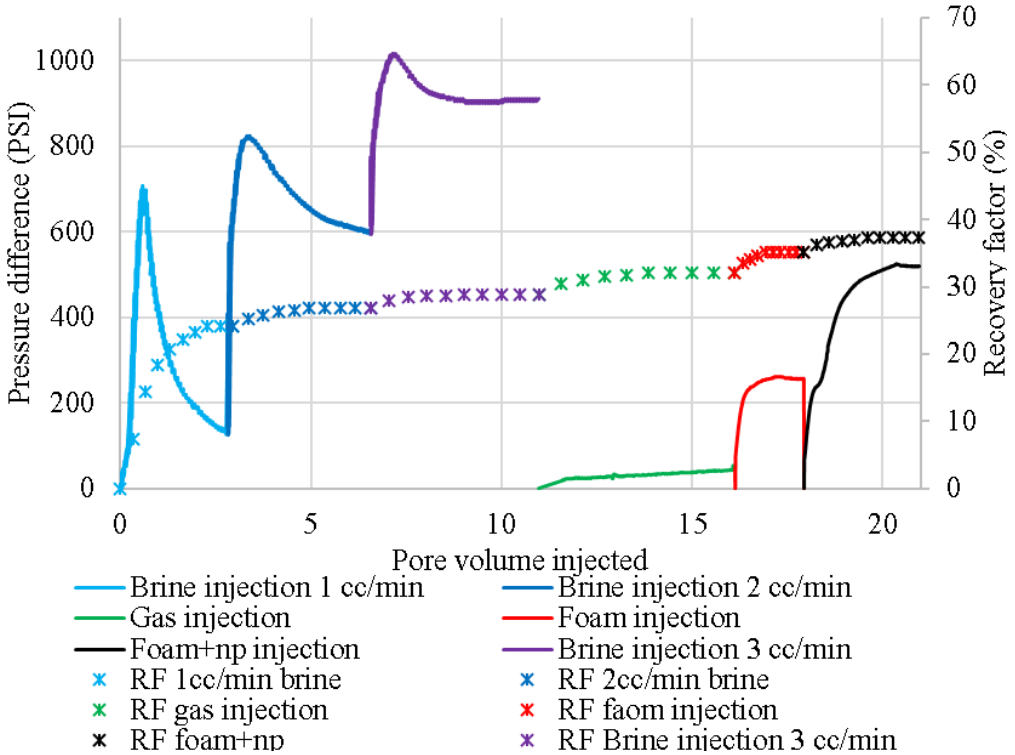

Figure 40. N_2 application Berea core flooding experiment results dP, RF vs PV

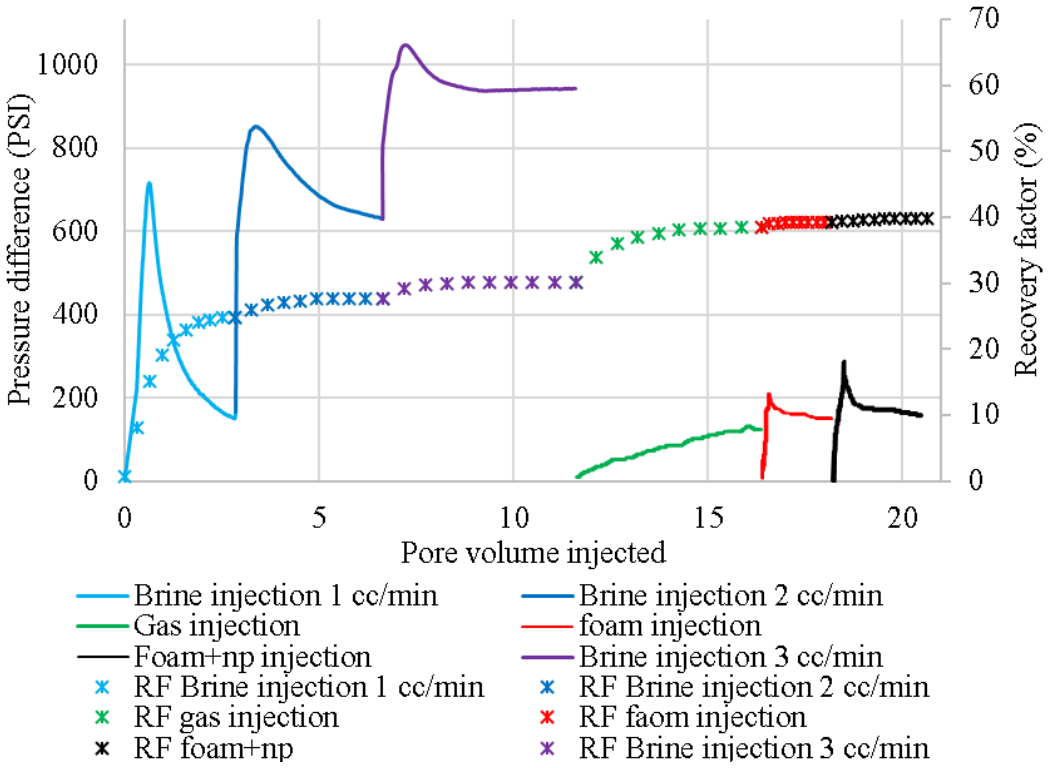

Figure 41. CO_2 application Berea core flooding experiment results dP, RF vs PV

4.3.2. *Indiana core sample flooding result*

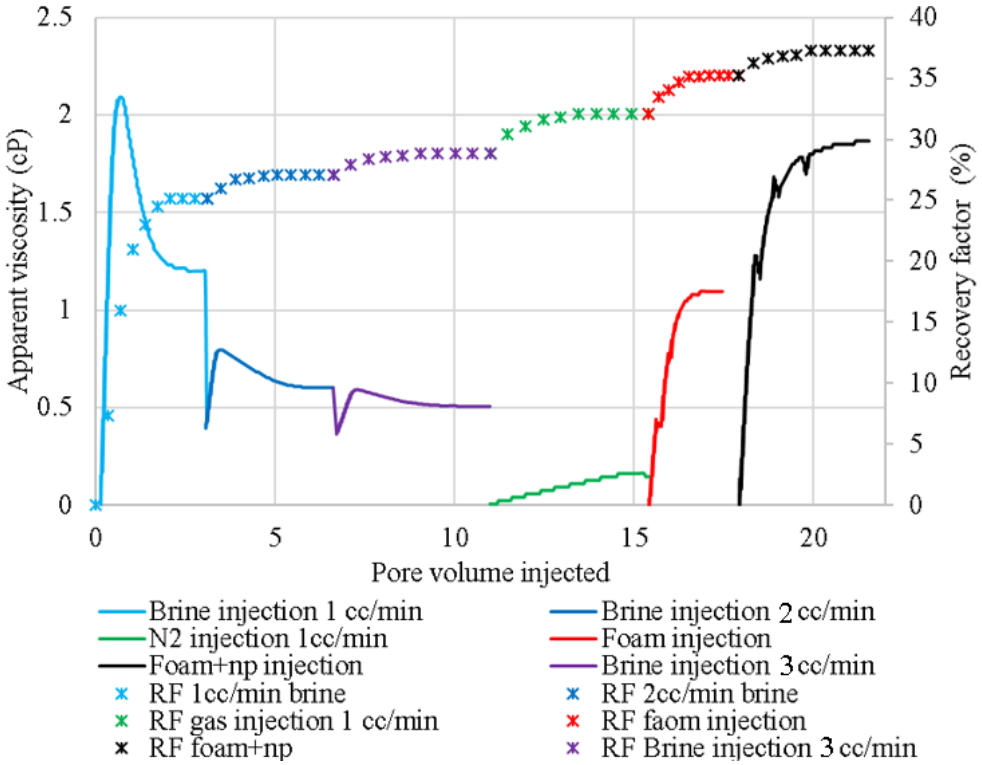

Figure 42. N_2 application Indiana core flooding experiment results apparent viscosity and RF vs PV

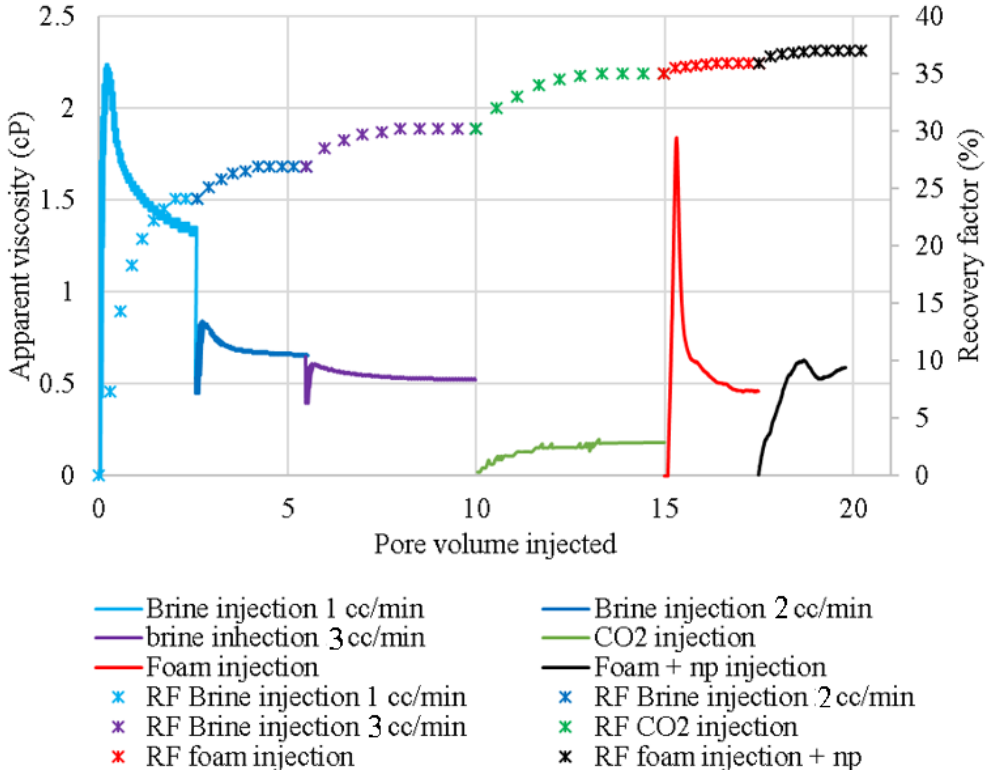

Figure 43. CO_2 application Indiana core flooding experiment results apparent viscosity and RF vs PV

Table 9. Indiana core flooding recovery factor increment comparison table

	RF	
	N_2	CO_2
Water flooding 1cc/min	25.1	24.13
Increment	*+2*	*+2.77*
Water flooding 2cc/min	27.1	26.9
Increment	*+1.7*	*+3.33*
Water flooding 3cc/min	28.8	30.23
Increment	*+3.33*	*+4.77*
Gas flooding 1c/min	32.13	35
Increment	*+3.07*	*+0.9*
Foam flooding 1cc/min	35.2	.35.9
Increment	*+2.1*	*+1.1*
Foam np flooding 1cc/min	37.3	37

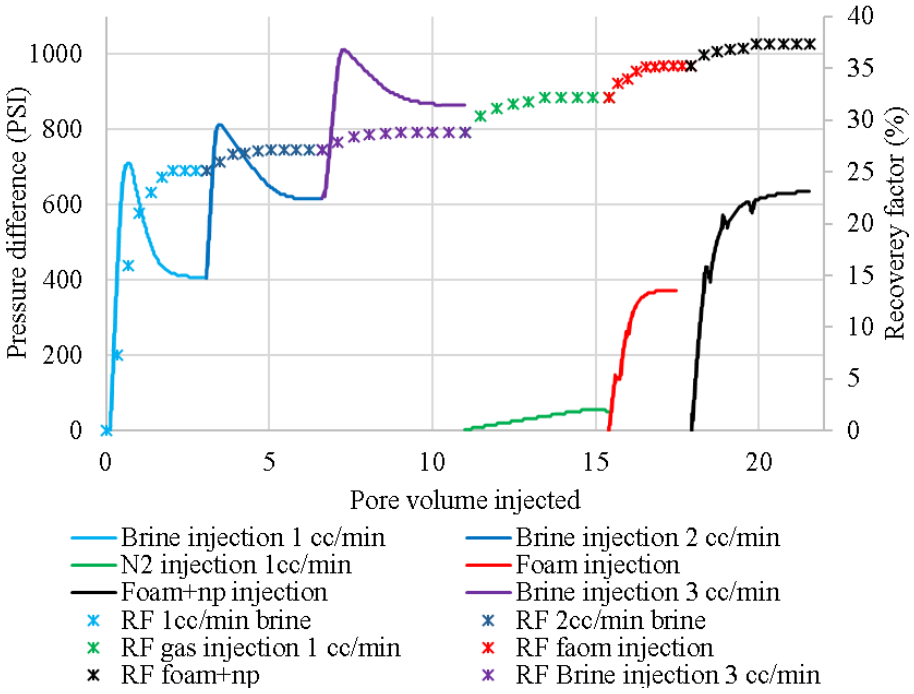

Figure 44. N_2 application Indiana core flooding experiment results dP, RF vs PV

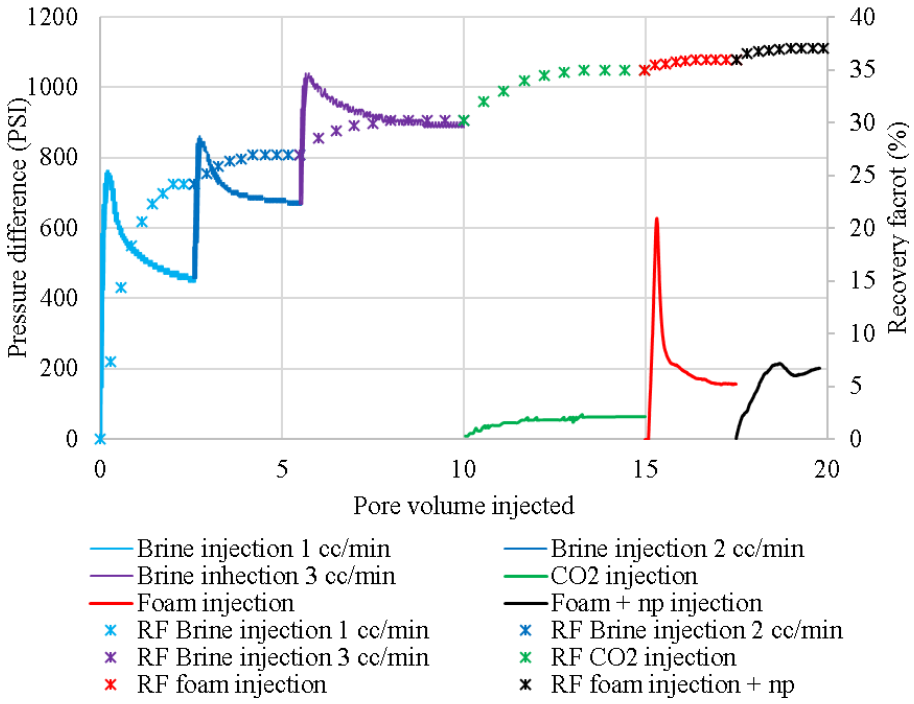

Figure 45. CO_2 application Indiana core flooding experiment results dP, RF vs PV

5. DISCUSSION

The work was conducted to compare the viability of N_2 and CO_2-based foams flooding formulations in the "X" oilfield. Four key aspects influencing foam behavior, and by extension, enhanced oil recovery outcomes, were highlighted: (1) mechanical properties of foam under atmospheric conditions, (2) mechanical properties of foam in porous media, (3) impact of lithology on EOR performance, (4) performance of foam boosting additives. Differences observed between CO_2 and N_2 foam performance highlight the features of each type of foam which should be considered before application as EOR technique.

5.1. Mechanical properties of foam under atmospheric conditions:

5.1.1. *Foam column stability*

According to the measured data, the CO_2-generated foam's half-life is significantly less than that of the N_2-generated foam. Essentially, under the same conditions, the carbon dioxide-based foams decomposed far faster than the nitrogen-based ones. This experimental finding aligns with a comparison found in the literature: Compared to N_2-foam, CO_2-foam is significantly less stable (has a shorter lifetime) for a given surfactant. In accordance with the fact that CO_2 has a significantly higher solubility in the aqueous phase (about one to two orders of magnitude greater than N_2), Farajzadeh et al. discovered that the half-life of a foam made from CO_2 was significantly less than that of a foam made from N_2 under similar conditions [42].

The stability of foams is mainly governed by the strength of the very thin liquid films (lamellae) and the liquid-draining rate from the foam films. As foam is produced, liquid will drain from the lamellae under the influence of capillary and gravitational forces. Liquid from the films is pushed into the Plateau border channels through gravity and capillary suction [43], leading to the gradual thinning of the lamellae. The disjoining pressure, or the forces that separate the

liquid films, falls off as the films become thinner. In the end, the films burst; there's nothing to keep them apart but the distance, which is no longer sustainable.

5.1.2. *Foam heterogeneity effects*

Experimentally, foam generated exiting coreflood tests with CO_2 was observed to contain larger, more heterogeneous bubbles, whereas N_2-derived foam consisted of smaller, more uniform bubbles (Figure 28).

This distinction can be explained by capillary pressure (P_c) effects described by the Young–Laplace equation:

$$P_c = \frac{2\gamma}{r} \quad (1)$$

where:

γ - is surface tension;

r – is radius of single bubble;

Thus, smaller bubbles have a greater internal pressure (Laplace pressure), and as a result, their liquid films are stronger and they are much more resistant to coalescence [48], additionally , reports show that sub-millimeter bubbles are stable orders of magnitude longer than multi-millimeter bubbles. In contrast, large bubbles have lower P_c, resulting in their films being relatively more susceptible to rupture and gas can diffuse from small high-pressure bubbles into larger low-pressure bubbles (Ostwald ripening) [49]. As a matter of fact, foams with wide-range bubble size distributions undergo coarsening more quickly, as larger P_c disparities drive gas transfer, while a more monodisperse (homogeneous) bubble size distribution slows down coarsening and increases foam stability [50]. Moreover, the enhanced solubility of CO_2 in the aqueous phase promotes the diffusion of gas and growth of bubbles in the foam coarsening of CO_2 foams [46]. Thus, the fine, high-P_c bubbles of the N_2 foam remain relatively stable (against coalescence and coarsening), while the larger, low-P_c CO_2 bubbles are prone to merging and growing, in agreement with the observations of differences in bubble size and foam stability.

Neighboring bubbles merge together, leading to larger bubbles and overall foam collapse [44]. Classical foam decay involves liquid drainage-induced film thinning followed by film breakage and bubble coalescence [44]. These processes occur in both CO_2 and N_2 foams, but their rates can differ depending on gas properties.

5.2. Mechanical properties in porous media of "X-oilfield"

To investigate how CO_2 an N_2 foam flooding work in porous media, the two cores collected from the field were investigated in core flooding experiments. In these low-perm pores, it is conjectured that CO_2 foam could not sustain a continuous lamella structure: gas threads quickly reconnect into continuous slugs, causing premature channeling through preferential pathways as evidenced by only ~1.6 cP apparent viscosity reached. By contrast, the stronger N_2 foam maintained a dispersed bubble morphology that substantially resisted flow ~4.8 cP, creating an effective gas-blocking network that diverted flow into unswept regions. From the apparent viscosity change profile, it is reasonable to assume that CO_2 foam degradate approaching 1.5 cP effective viscosity, as if reaching the critical capillary pressure. If the foam is not resilient, Kam & Rossen's population-balance model predicts foam collapse back to a single-phase gas flow[53]. Indeed, X-ray CT visualizations by Farajzadeh et al. (2009) show that when foam lamellae destabilize, gas fingers through the rock, bypassing oil [42]. Thus, N_2 foam's finer texture and more robust lamella propagation yield superior pore-scale trapping and sweep, whereas CO_2 foam remains too weak to invade and exit narrow throats without rupturing, resulting in poor sweep and a limited incremental oil recovery of 2.45 %.

5.3. Impact of lithology on EOR performance

In order to evaluate the effect of lithology on EOR performance, the identical foam flooding design as for the granitoid "X-field" cores were employed for the sandstones in Indiana and Berea outcrop cores. Although the Indiana and Berea cores exhibit similar filtration properties, their oil recovery and apparent viscosity profiles during foam flooding did not differ markedly. The additional oil recovery in both sandstone samples was 0.7 % for Berea and 0.9 % for Indiana with CO_2 foam, and 3.08 % and 3.07 % with N_2 foam, respectively. While the apparent viscosity profiles varied

somewhat, the general trend remained the same. For instance, the stabilized apparent viscosity during CO_2 foam flooding in Berea was around 1.1 cP (with a peak of 1.7 cP), whereas in Indiana it stabilized at approximately 0.5 cP (with a peak of 1.8 cP) (Figure 46).

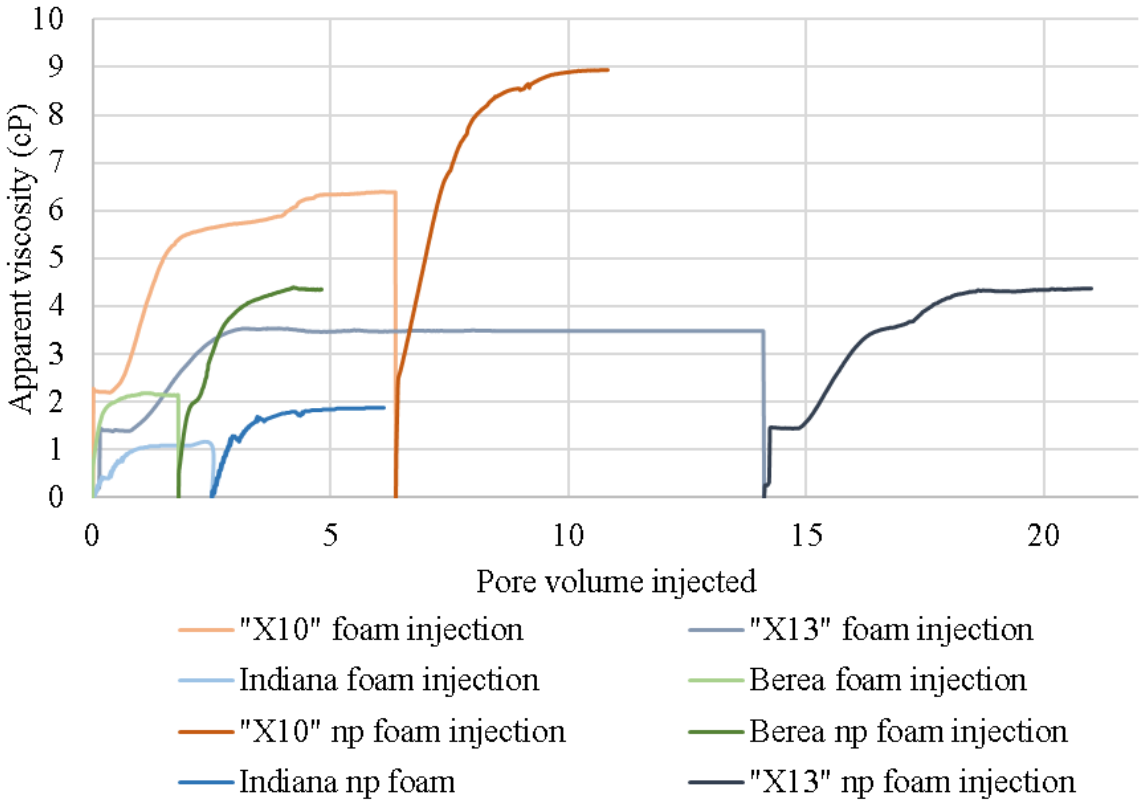

Figure 46. N_2 foam flooding apparent viscosity comparison

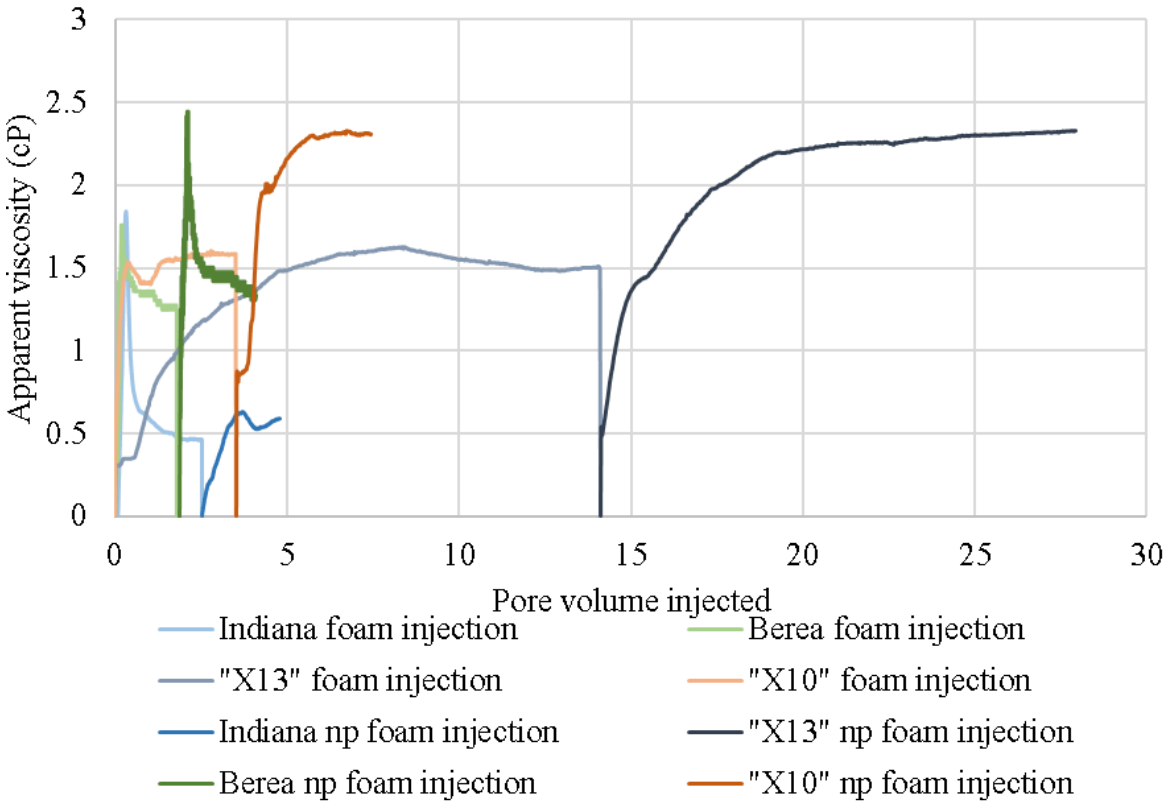

Figure 47. CO_2 foam flooding apparent viscosity comparison

In contrast, flooding tests on the "X-oilfield" granitoid cores displayed slightly different yet more consistent patterns. The recovery factors achieved in the "X-10" core was 1.8 % for CO_2 foam and 5.7 % for N_2 foam, while the "X-13" core yielded 3.1 % for CO_2 and 10.6 % for N_2 (Figure 48). It appears that foam performance was generally more effective in the "X" cores, likely due to their higher heterogeneity and correspondingly greater need for mobility control. Additionally, the apparent viscosity profiles in the "X" cores were more uniform, lacking the pronounced peaks seen in the outcrop cores-possibly another consequence of the granitoid samples' complex pore structure. Notably, the absolute apparent viscosities for CO_2 foam in both "X-10" and "X-13" remained below 2 cP, yet for N_2 foam, the apparent viscosity rose to 6 cP in "X-10" and only 1.1 cP in "X-13," indicating that permeability can strongly influence foam flooding behavior.

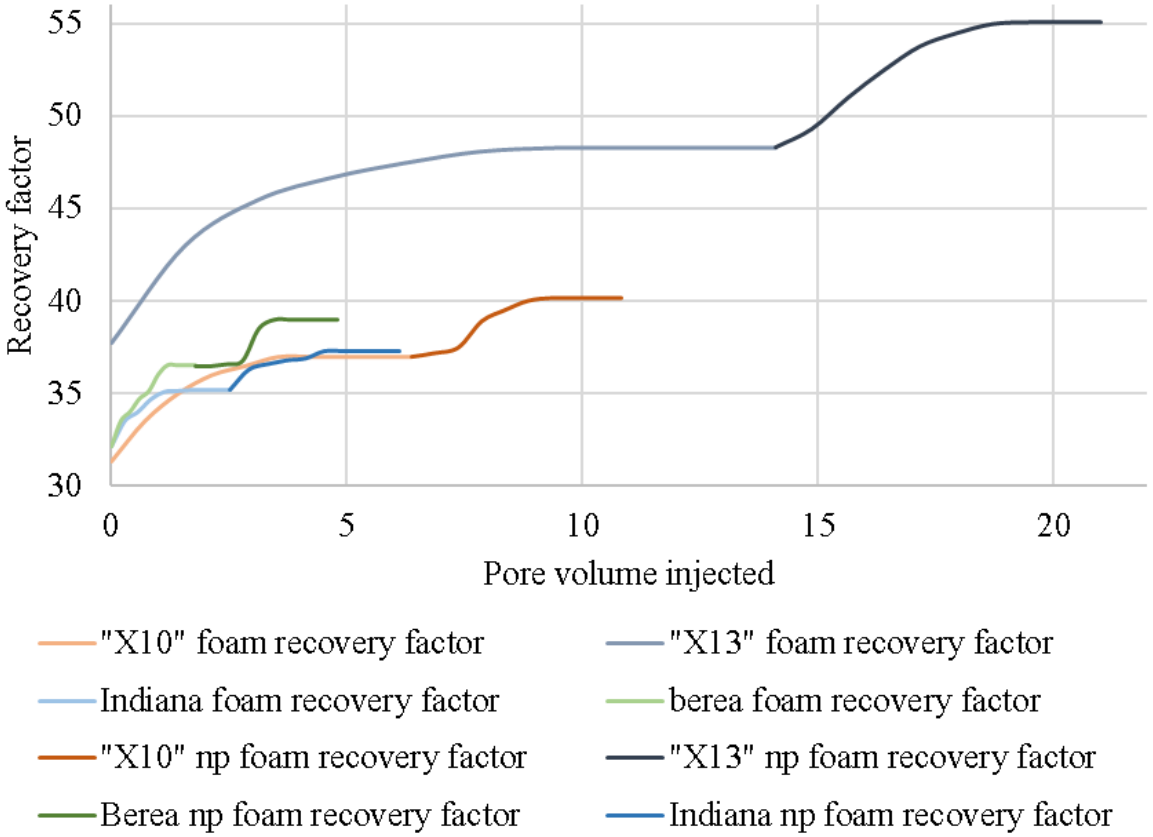

Figure 48. N_2 foam flooding recovery factor comparison for foam flooding

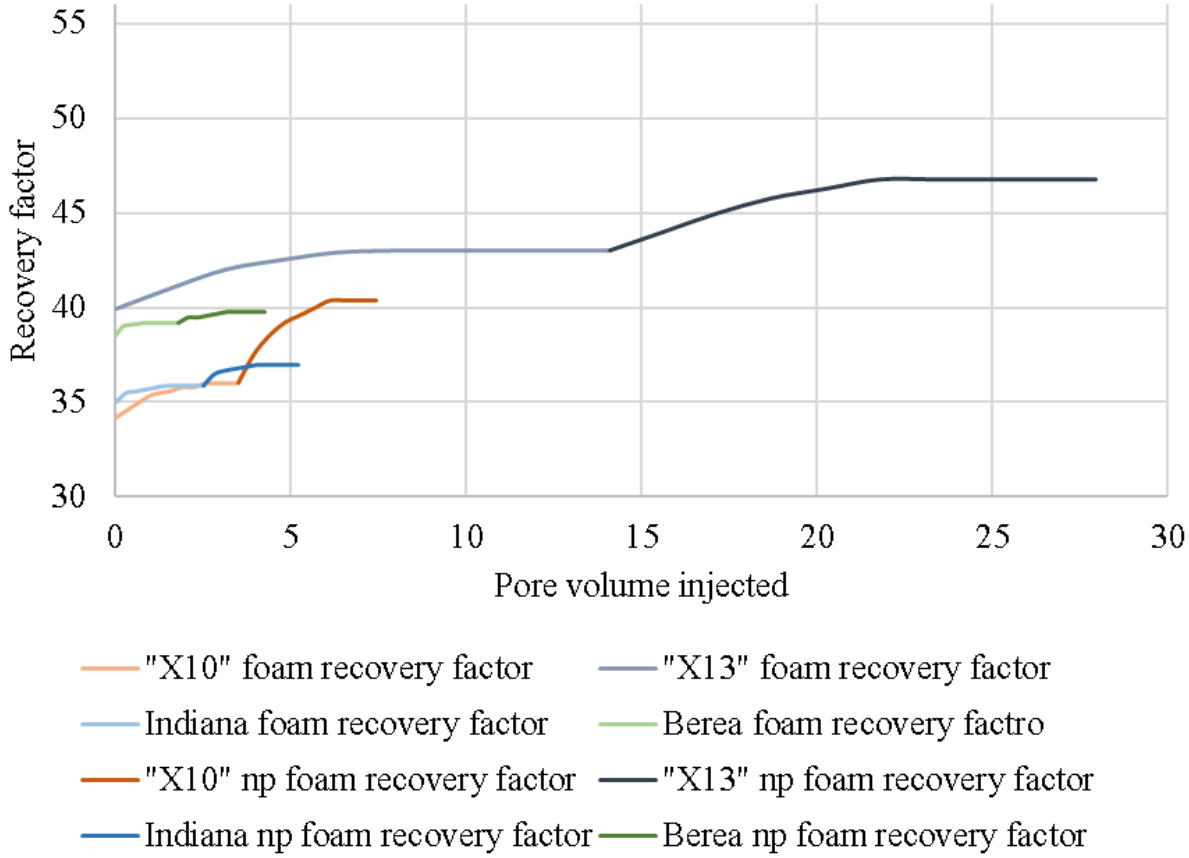

Figure 49. CO_2 foam flooding recovery factor comparison for foam flooding

5.4. Foam flooding additives

In order to investigate the effect of additives on foam flooding efficiency, an additional flooding test was carried out after the baseline (conventional) foam flooding. The only difference from the initial experiment was the addition of 0.1 % silica nanoparticles to the foam solution. By strengthening foam films and boosting their viscoelasticity, the nanoparticles improved the foam's ability to control mobility and make it more resilient against collapse [53]. By adding these nanoparticles, average oil recovery rose to about 5.05 % for N_2 foam flooding and 4.1 % for CO_2 foam flooding, showing that nanoparticles improve recovery for both types of foam.

However, this modest improvement in oil recovery led to a considerable rise in apparent viscosity. Specifically, in the “X-10” core flooding tests, nanoparticle addition increased the apparent viscosity to 4.3 cP (a 33 % increase) for N_2 foam and 2.4 cP (a 37 % increase) for CO_2 foam. In the “X-13” core, the apparent viscosity rose to 9 cP (a 30 % increase) for N_2 foam and 2.2 cP (a 20 % increase) for CO_2 foam. Although nanoparticles present

a promising avenue for enhancing foam flooding performance, these results suggest that their application can lead to a steep surge in apparent viscosity-potentially exceeding what the core (and by extension, the reservoir) can accommodate under real-field conditions. Consequently, while nanoparticles offer clear benefits, a careful evaluation of potential drawbacks is crucial prior to large-scale deployment.

6. CONCLUSION

Various experiments were conducted to investigate the ability of foam application to improve oil recovery at the “X” oilfield. Experiments involved the investigation of bulk foam properties at atmospheric conditions and foam behavior during core flooding. A foam half-life test was conducted to estimate the most compatible solution that could be applied for flooding. Core flood experiments investigated the performance and potential mechanisms participating in the flooding process. Furthermore, the core flooding process was designed to investigate the role of different lithology and nanoparticle impacts on the flooding process. Based on the results of the experiments, the following conclusions were reached:

- Viable foam formulations were screened in foam bulk tests. The optimum concentration was determined as 0 % sodium chloride (NaCl), 0.25 % BIO-TERGE surfactant, and 0.1 % silica nanoparticles. The solution marginally demonstrated the longest foam half-time in comparison with other concentrations – 310 min.
- Regardless of the core sample or lithology tested, foam exiting the core in CO_2 flooding had a much coarser texture than N_2 foams.
- Regardless of the core sample or lithology tested, foam collected from the outlet line after CO_2 flooding is colored by oil color while bubbles collected after N_2 are white without a trace of oil. This indicates the tendency of CO_2 foam to chemically interact with the surrounding fluid.
- In bulk foam tests with 0.1 % BIO-TERGE surfactant and 0.1 % silica nanoparticles in 1 % NaCl, N_2 half-life was 16.6 % longer than CO_2 foam.
- A comparison of the N_2 and CO_2 foam flooding results demonstrate that N_2 foam is more efficient. Thus, the average increment in recovery reached after N_2 foam flooding applied at "X" core samples is 8.15 % and 3.08 % for outcrop core samples, while for CO_2 the values are 2.45 % and 0.8 % respectively.
- A comparison of the N_2 and CO_2 foam with silica nanoparticle flooding results demonstrates that N_2 foam is more efficient. Thus, the average increment in

recovery reached after N_2 foam flooding applied at "X" core samples is 5.05 % and 2.01 % for outcrop core samples, while for CO_2 the values are 4.1 % and 1 % respectively.

- A comparison of the foam flooding results demonstrates that “X” oilfield core samples have the potential for additional oil recovery by foam flooding.
- Comparing performance across lithologies, after N_2 foam with nanoparticles flooding, 17 % more additional oil was produced from “X” oilfield core samples in comparison with outcrop cores. CO_2 foam with nanoparticles flooding demonstrated 10.4 % more additional oil produced in “X” core samples than in outcrop core samples.
- The application of nanoparticles significantly improves foam efficiency. The addition of 0.1 % silica nanoparticles during CO_2 foam flooding increased the recovery factor by 2.5 % OOIP on average. Application of silica nanoparticles during N_2 foam flooding increased that parameter by 3.6 % of OOIP.
- High values of apparent viscosity reached during N_2 foam flooding with silica nanoparticles flooding experiments require careful consideration before field implementation, as the average apparent viscosity during N_2 foam with silica nanoparticles flooding reached a maximum of 9 cP.
- The average apparent viscosity during CO_2 foam with silica nanoparticles flooding reached a maximum of 2.4 cP, making the application of silica nanoparticles during foam flooding more plausible.
- While the N_2 foam core flooding results demonstrated better results in comparison with CO_2 foam, immiscible CO_2 gas flooding is more efficient than immiscible N_2 flooding. The average recovery factor for CO_2 gas flooding was 36.9 %, while the N_2 average gas flooding efficiency was 32.8 %.

7. FUTURE WORK

For better understanding of complex problem foam mechanics and exceeding limitations of the current study, the next scope of investigation is proposed:

- Screen different surfactants (other than Bio-Terge) for foam flooding.
- Study the effect of different nanoparticles (other than silica nanoparticles) and concentrations for foam flooding.
- Repeat experiments with miscible gas and miscible foam flooding.
- Investigate foam diversion mechanisms.
- Simulation foam flooding experiments in commercial simulators.
- Pilot test foam flooding implementation at the oilfield in Kazakhstan where thief zones are identified.
- Investigate the effect of temperature on foam flooding efficiency.
- Study surfactant adsorption in core.
- Conduct the foam flooding experiment as a secondary recovery method.

REFERENCES

[1] Blunt, M., Fayers, F.J., Orr, F.M., 1993. Carbon dioxide in Enhanced Oil Recovery. Energy Conversion and Management 34, 1197–1204.

[2] Green, D.W., Willhite, G.P., 2018. . Enhanced Oil Recovery.

[3] Lake, L., Johns, R.T., Rossen, W.R., Pope, G.A., 2014. . Fundamentals of Enhanced Oil Recovery.

[4] Sheng, J.J., 2011. Introduction. Modern Chemical Enhanced Oil Recovery 1–11.

[5] Sheng, J.J., 2013. Surfactant enhanced oil recovery in Carbonate Reservoirs. Enhanced Oil Recovery Field Case Studies 281–299.

[6] Mandal, A., 2015. Chemical Flood Enhanced Oil Recovery: A Review. International Journal of Oil, Gas and Coal Technology 9, 241.

[7] Godec, M., 2014. . Acquisition and development of selected cost data for saline storage and Enhanced Oil Recovery

[8] Farajzadeh, R., Andrianov, A., Zitha, P.L., 2009. Foam assisted enhanced oil recovery at Miscible and immiscible conditions. Kuwait International Petroleum Conference and Exhibition.

[9] Rossen, W.R., 2017. Foams in enhanced oil recovery. Foams 413–464.

[10] Vikingstad, A.K., Aarra, M.G., 2009. Comparing the static and dynamic foam properties of a fluorinated and an alpha olefin sulfonate surfactant. Journal of Petroleum Science and Engineering 65, 105–111.

[11] Zeng, Y., Miller, C. A., & Mohanty, K. K., 2018. Improving foam performance for mobility control by modifying surfactant headgroups. Energy & Fuels, 32(6), 6238-6247.

[12] Li, R.F., Yan, W., Liu, S., Hirasaki, G.J., Miller, C.A., 2010. Foam mobility control for surfactant enhanced oil recovery. SPE Journal 15, 928–942.

[13] Dogah, B., Atashbari, V., Ahmadi, M., Sheets, B., 2021. Enhanced oil recovery using CO_2 in Alaska. Geosciences 11, 98.

[14] Blaker, T., Aarra, M.G., Skauge, A., Rasmussen, L., Celius, H.K., Martinsen, H.A., Vassenden, F., 2002. Foam for gas mobility control in the Snorre Field: The FAWAG project. SPE Reservoir Evaluation & Engineering 5, 317–323.

[15] Janssen, M.T., Mutawa, A.S., Pilus, R.M., Zitha, P.L., 2019. Foam-assisted chemical flooding for enhanced oil recovery: Effects of slug salinity and drive foam strength. Energy & Fuels 33, 4951–4963.

[16] Denney, D., 2013. Foam-eor pilot: Mature volatile-oil reservoir under miscible-gas injection. Journal of Petroleum Technology 65, 117–119.

[17] Yu, H., 2023. Research status and development trend of air-foam EOR technology. OALib 10, 1–13.

[18] Bello, A., Ivanova, A., Cheremisin, A., 2023. Foam Eor as an optimization technique for GAS EOR: A comprehensive review of laboratory and field implementations. Energies 16, 972.

[19] Jonas, T.M., Chou, S.I., Vasicek, S.L., 1990. Evaluation of a CO_2 foam field trial: Rangely Weber Sand unit. SPE Annual Technical Conference and Exhibition.

[20] Henry, R., Fisher, D., Pennell, S., Honnert, M., 1996. Field test of foam to reduce CO_2 cycling. Proceedings of SPE/DOE Improved Oil Recovery Symposium.

[21] Ocampo, A., Restrepo, A., Cifuentes, H., Hester, J., Orozco, N., Gil, C., 2013. Successful foam EOR pilot in a mature volatile oil reservoir under miscible gas injection. In International Petroleum Technology Conference (pp. IPTC-16984). IPTC.

[22] D’Souza, D., Cochram, J., Chabert, M., Delamaide, E., 2017. Foam Enhances CO_2 EOR Performance. Amer. Oil & Gas Reporter

[23] Blaker, T., Aarra, M.G., Skauge, A., Rasmussen, L., Celius, H.K., Martinsen, H.A., Vassenden, F., 2002a. Foam for gas mobility control in the Snorre Field: The FAWAG project. SPE Reservoir Evaluation & Engineering 5, 317–323.

[24] Skauge, A., Aarra, M.G., Surguchev, L., Martinsen, H.A., Rasmussen, L., 2002. Foam-assisted WAG: Experience from the Snorre Field. Proceedings of SPE/DOE Improved Oil Recovery Symposium.

[25] Friedmann, F., Smith, M.E., Guice, W.R., Gump, J.M., Nelson, D.G., 1994. Steam-foam mechanistic field trial in the midway-sunset field. SPE Reservoir Engineering 9, 297–304.

[26] Hoefner, M.L., Evans, E.M., 1995. CO_2 foam: Results from Four developmental field trials. SPE Reservoir Engineering 10, 273–281.

[27] Lemmon, E.W., Huber, M.L., 2004. Thermodynamic properties ofn-dodecane. Energy & Fuels 18, 960–967.

[28] Huber, M.L., Laesecke, A., Perkins, R., 2004. Transport properties ofn-dodecane. Energy & Fuels 18, 968–975.

[29] Mao, Y., Raza, M., Wu, Z., Zhu, J., Yu, L., Wang, S., Zhu, L., Lu, X., 2020. An experimental study of N-Dodecane and the development of an improved kinetic model. Combustion and Flame 212, 388–402.

[30] Крупин, А. А., 2011. Нефтегазоносность гранитной интрузии месторождения «Оймаша». Научные труды НИПИ Нефтегаз ГНКАР, (2), 11-17.

[31] Попков, В. И., Попков, И. В., Крупин, А. А., 2020. Новые данные о строении резервуара нефтяной залежи в гранитном массиве и перспективы доразведки месторождения Оймаша. Булатовские чтения, 1, 155-161.

[32] Попков, В. И., Попков, И. В., 2019. Структурно-формационная характеристика верхнепалеозойских отложений запада Туранской плиты. Геология, география и глобальная энергия, 4, 9-17.

[33] KazNIPImunaigas branch of KMG Engineering LLP STANDARD AND SPECIAL CORE STUDIES FROM EVALUATION AND PRODUCTION WELLS

[34] Ларичев, В. В., Попков, В. И., Попков, И. В. 2020. Гидрохимический облик пластовых вод месторождения оймаша. Геология, география и глобальная энергия, (2), 51-59

[35] Farajzadeh, R., Andrianov, A., Krastev, R., Hirasaki, G.J., Rossen, W.R., 2012. Foam–oil interaction in porous media: Implications for foam assisted enhanced oil recovery. Advances in Colloid and Interface Science 183–184, 1–13.

[36] Kovscek, A.R., Radke, C.J., 1993. . Fundamentals of foam transport in porous media.

[37] Sun, Q., Zhang, N., Li, Z., Wang, Y., 2016. Nanoparticle-stabilized foam for mobility control in enhanced oil recovery. Energy Technology 4, 1084–1096.

[38] Cui, X., Liu, Z., Cui, P., & Du, D. (2023). A novel methodology for measurement of the diffusion coefficient between CO_2 and oil based on quantification of the oil droplet swelling behavior. Colloids and Surfaces A: Physicochemical and Engineering Aspects, 656, 130485.

[39] Wang, J.-L., Song, Z.-H., Li, L.-J., Yang, L.-L., Wang, Q.-Y., Chou, I.-M., Pan, Z.-Y., 2022. Integration of a fused silica capillary and in-situ Raman spectroscopy for investigating CO_2 solubility in N-dodecane at near-critical and supercritical conditions of CO_2. Petroleum Science 19, 3124–3133.

[40] Guan, J., Liang, L., Zhao, Y., Sun, N., Lu, W., Zhen, Y., 2023. Study on screening and evaluation of foam drainage agents for gas wells with high temperature and high pressure. ACS Omega 8, 7940–7949.

[41] Bello, A., Ivanova, A., Cheremisin, A., 2022. Enhancing N_2 and CO_2 foam stability by surfactants and nanoparticles at high temperature and various salinities. Journal of Petroleum Science and Engineering 215, 110720.

[42] Farajzadeh, R., Andrianov, A., Bruining, H., Zitha, P. L. 2009. Comparative study of CO_2 and N_2 foams in porous media at low and high pressure− temperatures. Industrial & Engineering Chemistry Research, 48(9), 4542-4552.

[43] Sheng, J. J. 2013. Enhanced oil recovery field case studies. Gulf professional publishing.

[44] Krishnan, P., Zhang, B., Anas, A. R., Cheng, Z., Mannan, M. S. 2017. Modeling the blanketing and warming effect of high expansion foam used for LNG vapor risk mitigation.

[45] Hanamertani, A.S., Saraji, S., Piri, M., 2023. A comparative investigation of the effect of gas type on foam strength and flow behavior in tight carbonates. Chemical Engineering Science 276, 118798.

[46] Vavra, E., Bai, C., Puerto, M., Ma, K., Mateen, K., Hirasaki, G.J., Biswal, S.L., 2023. Effects of velocity on N_2 and CO_2 foam flow with in-situ capillary pressure measurements in a high-permeability homogeneous sandpack. Scientific Reports 13.

[47] Farajzadeh, R., Vincent-Bonnieu, S., Bourada Bourada, N., 2014. Effect of gas permeability and solubility on foam. Journal of Soft Matter 2014, 1–7.

[48] Pagureva, N., Tcholakova, S., Rusanova, K., Denkov, N., & Dimitrova, T. (2016). Factors affecting the coalescence stability of microbubbles. Colloids and Surfaces A: Physicochemical and Engineering Aspects, 508, 21-29.

[49] Voorhees, P.W., 1985. The theory of Ostwald ripening. Journal of Statistical Physics 38, 231–252.

[50] Yu, W., Zhou, X., 2022a. Experimental and modeling study of foam coarsening kinetics in Porous Media. Frontiers in Energy Research 10.

[51] Polikarpov, E., Albrecht, K.O., Page, J.P., Malhotra, D., Koech, P.K., Cosimbescu, L., Gaspar, D.J., 2019. Critical fuel property evaluation for potential gasoline and diesel biofuel blendstocks with low sample volume availability. Fuel 238, 26–33.

[52] Wang, M., Yang, S., Li, J., Zheng, Z., Liu, Q., Wen, J., Zhang, Y., 2020. Pressure-sensitive characteristics of high-pour-point live oil and quantitative analysis of Composition Change. Journal of Petroleum Science and Engineering 193, 107430.

[53] Xu, Z., Li, B., Zhao, H., He, L., Liu, Z., Chen, D., Yang, H., Li, Z., 2020. Investigation of the effect of nanoparticle-stabilized foam on EOR: Nitrogen foam and methane foam. ACS Omega 5, 19092–19103.

[54] Dasari, S.R., Goud, V.V., 2014. Effect of pre-treatment on solvents extraction and physico-chemical properties of castor seed oil. Journal of Renewable and Sustainable Energy 6.

[55] Amro, M., Finck, M. and Jaeger, P. (2015) 'Foams at elevated pressure in Eor', SPE Middle East Oil & Gas Show and Conference

[56] Alali, R. *et al.* (2023) 'Effect of carbon dioxide injection on limestone permeability damage induced by alumina nanoparticles for enhanced oil recovery applications', *Applied Sciences*, 13(13), p. 7446. doi:10.3390/app13137446.